CZECH TECHNICAL UNIVERSITY IN PRAGUE
Faculty of Mechanical Engineering
Department of Energy Engineering

A design of an experimental facility for the coarse water droplets measurement

Master Thesis

Study Programme: N2301 – Mechanical Engineering
Branch of study: 3907T002 – Power Engineering

Thesis advisor: Ing. Ondřej Bartoš, Ph.D.

Bc. Jiří Janoušek

Prague 2016

Assignment

Statutory declaration

I assure that my thesis "*A design of an experimental facility for the coarse water droplets measurement*" is a result of my personal work and that no other than the indicated aids have been used for its completion. Furthermore, I declare that all quotations and statements that have been inferred literally or in a general manner from others are clearly marked. The work has not been used, neither completely nor in parts, to achieve academic grading or being published elsewhere.

In Prague, 10.6. 2016 _____

Summary page

Author's name:	Jiří Janoušek

Title of thesis:	A design of an experimental facility for the coarse water droplets measurement
Czech title:	Návrh experimentálního zařízení pro výzkum hrubé vodní disperze
Academic year:	2015/2016
Department:	Department of Energy Engineering
Advisor:	Ing. Ondřej Bartoš, Ph.D.
Bibliographic data:	Number of pages: 79 Number of figures: 40 Number of tables: 12 Number of appendices: 2
Keyword:	photogrammetry, granulometry, steam turbines, coarse droplets, wind tunnels
Klíčová slova:	fotogrammetrie, granulometrie, parní turbíny, sekundární kapky, aerodynamické tunely

Abstract: The thesis is focused on problems of polydisperse systems, particularly on coarse droplets in steam turbines. The necessary background is introduced in the search part. In the practical part, a special program for the analysis of images containing polydisperse systems was developed. Its analysing capability was verified on several images with different polydisperse systems. The program also provides granulometric characteristics of the system. A design of a wind tunnel for simulating the tearing away process of coarse droplets in steam turbines was performed in the other practical part. The tearing away process will be captured by the photogrammetric probe that has been developed within the research at the Department of Energy Engineering. It will help to verify the probe's functionality.

Anotace: Diplomová práce je zaměřena na polydisperzní systémy, především na sekundární kapky v parních turbínách. Rešeršní část obsahuje základní informace k problematice. V praktické části byl vytvořen program pro automatické vyhodnocení obrazu polydisperzního systému. Jeho funkčnost byla ověřena na několika snímcích různých polydisperzních systémů. Program vyhodnocuje i granulometrické charakteristiky systému. Druhým bodem praktické části byl návrh aerodynamického tunelu, ve kterém bude docházet k odtrhávání kapek vody, čímž bude simulován proces vzniku sekundárních kapek v parních turbínách. Odtrhávání bude zachycováno fotogrammetrickou sondou, která je vyvíjena v rámci širšího výzkumu na Ústavu Energetiky, což přispěje k ověření její funkčnost před aplikací přímo v turbíně.

Acknowledgements

First, I would like to thank my advisor Ing. Ondřej Bartoš, Ph.D. for supervising my thesis and for his valuable recommendations and advices. I would also like to thank D.Sc. (Tech.) Jari Backman from Lappeenranta University of Technology who helped me during writing the theoretical part while I was an exchange student in Finland.

Table of Contents

List of symbols....8
1 Introduction....11
2 Disperse systems....12
2.1 Aerosols....13
2.2 Properties of polydisperse systems....13
2.3 Analysis of polydisperse systems....14
2.3.1 Determination of system distribution....14
2.3.2 Mathematical models....19
2.3.2.1 Rosin-Rammler distribution....19
2.3.2.2 Log-normal distribution....20
2.3.3 Determination of the particle diameter....20
2.3.4 Basic statistical evaluation – mean, median, mode....24
3 Examples of measuring methods....26
3.1 Sampling of the system of particles....26
3.2 Sieving....27
3.3 Sedimentation....27
3.4 Laser diffraction....28
3.5 Microscopy....29
3.6 Photogrammetry....31
4 Measurements in steam turbines....34
4.1 Wet steam in steam turbines....34
4.1.1 Condensation....35
4.1.1.1 Heterogeneous....35
4.1.1.2 Homogeneous....35
4.2 Wetness measurements....35
4.2.1 Thermodynamic methods....36
4.2.2 Specific measurements in wet steam....36
4.2.2.1 Fine droplets....36
4.2.2.2 Coarse droplets....38
4.3 Other measurements....39
5 Image evaluation....40
5.1 Calibration....40
5.2 Analysis of the glass powder....41
5.3 Analysis of ground coal....49
5.4 Suggestions for improvements....54
5.5 Conclusion....55
6 Design of the experimental wind tunnel....56
6.1 Wind tunnel background search....56
6.2 Objectives for a design of the wind tunnel....57
6.3 Description of the test facility....57
6.4 Basic calculation of the nozzle for air....58
6.5 Design elements....62
6.6 Specific design of the measuring chamber....62
6.6.1 Assembly....62
6.6.1.1 Description of the welding and assembling process....63

6.6.2 Specification of individual components....64
6.6.2.1 Nozzle shape....64
6.6.2.2 Base part....66
6.6.2.3 Sidewalls....68
6.6.2.4 Flanges....68
6.6.2.5 Housing tubes....68
6.6.2.6 Airfoil....69
6.6.2.7 Supporting pins....69
6.6.2.8 Supply tubes....69
6.6.2.9 Coupling pin....69
6.6.2.10 Glass windows....70
6.6.2.11 O-rings....70
6.6.2.12 Hoops of thrust rings....71
6.6.2.13 Fastening plates of thrust rings....71
6.6.2.14 Confuser....71
6.7 Strength calculations of the test section....72
6.7.1 Settling chamber....72
6.7.1.1 The tube of the settling chamber....72
6.7.1.2 Weld between the tube and cap....73
6.7.2 The connecting tube....73
6.7.3 Flange joint....74
6.8 Conclusion....74
7 Conclusion....75
Sources....77
List of appendices....80

List of symbols

symbol	unit	property
a, b	µm	particle size parameters
c	--	compression
c^*	m/s	critical flow speed
c_p	kJ/(kg·K)	specific heat capacity at constant pressure
c_v	kJ/(kg·K)	specific heat capacity at constant volume
D_w	mm	weld outer diameter
$d_{[0,1]}$	µm	number median diameter
$d_{[1,0]}$	µm	number length mean
$d_{[2,0]}$	µm	number surface mean
$d_{[3,0]}$	µm	number volume or weight mean
$d_{[3,2]}$	µm	surface area mean diameter (Sauter diameter)
$d_{[4,3]}$	µm	mass mean diameter (De Brouckere diameter)
Δd_i	µm	size interval i
d_a	µm	particle diameter based in area
d_g	µm	geometric mean diameter
d_i	µm, mm	middle diameter of the size interval i, inner diameter
$d_{\bar{m}}$	µm	average mass diameter
d_p	m, µm	particle diameter
d_{pr}	µm	particle diameter based on perimeter
d_s	mm	O- ring diameter
$d_{\bar{s}}$	µm	average surface diameter
d_w	mm	weld inner diameter
dd_p	µm	differential interval of size of particles
df	--	fraction of the total number of particles
F	--; N	cumulative distribution function; force
F_{RR}	--	cumulative distribution function of Rosin-Rammler distribution
f_{ab}	--	frequency of particles between particle sizes a and b (frequency function)
f_{RR}	--	frequency function of Rosin-Rammler distribution
f_{ln}	--	frequency function of log-normal distribution
f_i	--/µm	fraction of particles in the size interval i
g	m/s^2	gravitational acceleration
h	kJ/kg	specific enthalpy
h^*	kJ/kg	specific enthalpy at critical conditions
h_i	--/µm	number or fraction of particles per unit of the size interval i
L	m	length

l	mm	groove depth for an O-ring
I	W/m^2	light intensity
I_0	W/m^2	original light intensity
k	--	index; safety factor
M	--	Mach number
M_{in}	--	inlet Mach number
M_{out}	--	outlet Mach number
M_t	--	Mach number in the throat
$\dot{m}^*$	kg/s	critical mass flow
m	kg	mass
m_i	kg, g	mass of all particles in size interval i
m_l	kg, g	mass of liquid
m_m	kg, g	mass of mixture
N	--	total number of particles
n	--	constant
n_i	--	number of particles in the size interval i
Δp	--	pressure difference
p	Pa	pressure
p^*	Pa	critical pressure
p_{in}	Pa	inlet pressure
p_{out}	Pa	outlet pressure
p^*_{out}	Pa	critical outlet pressure
p_s	Pa	static pressure
p_t	Pa	total pressure; pressure in the throat
Q	--	extinction factor
r	kJ/(kg·K); mm	specific gas constant; radius
r_p	µm	particle radius
S	–; mm^2	complementary cumulative distribution function; area
S^*	mm^2	critical area
S_{RR}	--	complementary cumulative distribution function of Rosin-Rammler distribution
s	mm	thickness
s_i	µm^2	surface of all particles in size interval i
T	K	temperature
T^*	K	critical temperature
t	s	time
V	m^3	volume
v	m/s	settling velocity; flow velocity
v^*	m^3/kg	critical specific volume

v_{in}	m/s	inlet velocity
v_{out}	m/s	outlet velocity
v_t	m/s	velocity in the throat
Y	--	wetness
α	--	constant
α_t	--	coefficient for a groove weld
β	--	critical pressure ratio
ζ	--	coefficient
η_f	Pa·s	fluid dynamic viscosity
κ	--	Poisson constant
ρ	kg/m^3	density; density of wet steam; flow density
ρ'	kg/m^3	liquid density on the saturation line
ρ''	kg/m^3	vapour density on the saturation line
ρ_p	kg/m^3	density of particles
ρ_f	kg/m^3	fluid density
σ_g	--	geometric standard deviation
σ_a	N/mm^2	axial stress
σ_m	N/mm^2	modified tensile stress
σ_p	N/mm^2	permissible stress
σ_r	N/mm^2	radial stress
σ_t	N/mm^2	tangential stress
σ_{tn}	N/mm^2	tensile stress
σ_v	N/mm^2	equivalent tensile stress
σ_y	N/mm^2	yield strength

1 Introduction

There have been unceasing efforts to improve efficiencies of machines. In case of machines consuming energy, the goal is to reduce their energy demands. Machines used for the energy production has been improving so that people gain as much energy as possible. In both cases, efforts eventually lead to savings of energy sources and subsequently financial savings.

A steam turbine, as a representative of machines producing energy, has been improving for identical reasons. Contemporary research of steam turbines extensively concerns with thermodynamic losses in low pressure stages of turbines. Due to the low pressure and temperature in these stages superheated steam, that is used in previous stages, turns into wet steam. Fine droplets in the wet steam probably start to accumulate on surfaces of turbine blades and later turn into water rivulets. The rivulets tear away from the blades of the fast-rotating turbine and create so called coarse droplets. These droplets cause not only energy losses but also the erosion of the blades. Moreover, the erosion process decreases the turbine performance over time as well as its reliability and lifetime.

There is an extensive research performing at the Energy Engineering Department of the Czech Technical University in Prague that is focused on processes related to coarse droplets. The main goal of the research is to find out where and how exactly coarse droplets form, tear away from blades, and affect them in the low pressure stages of steam turbines. The important information needed to be examined is the number of coarse droplets, their size and velocity after the tearing away.

Several physical principles were tested for measuring coarse droplets, but conditions of droplets occurrence were inconvenient for obtaining good results. Photogrammetry uses images captured by a camcorder or camera for determining shapes of projected objects as well as distances between them, and it is thought that it might be applied on coarse droplets. However, the concentration of coarse droplets is very low and thus the droplet occurs only on a few images of thousands that are taken.

For that reason, the first goal of the thesis was to devise a special computer program for an automatic image evaluation. Since all coarse droplets are not identical, they form a polydisperse system (system consisting of particles with different sizes). The program could be probably used for an identification of other polydisperse systems, too.

A few photographs direct from the low pressure stage of the steam turbine were taken within earlier activities of the ongoing research. However, their quality was poor and it was hard to evaluate them. Therefore, a photogrammetric probe that captured the images has been improved. In order to verify functionality of the probe before the application in the turbine, a wind tunnel for simulating and observing the tearing away process is needed. A design of such a wind tunnel was the other goal of the thesis.

2 Disperse systems

Any disperse system consists of a dispersion medium, in which a dispersed phase is. Dispersion medium is continuous and it can be gas, liquid or solid as well. The chemical composition of the dispersed phase can differ from the dispersion medium and it also can be solid, liquid or gas. The vast majority of disperse systems is a multi-constituent mixture. [2], [3]

Disperse systems can be divided according to many different points of view [2], [3]:

- according to a size of the particles of the disperse phase (linear size *d*)
  - coarse systems – $d_p > 10^{-6}$ m
  - colloidal systems – 10^{-6} m < $d_p < 10^{-9}$ m
  - fine systems (true solutions) – $d_p < 10^{-9}$ m
- according to a number of phases in the system
  - homogeneous systems – the dispersion medium and the dispersed phase are in the same phase
  - heterogeneous systems – the dispersion medium and the dispersed phase are separated by interface

    According to the combination of a dispersion medium and a dispersed phase, homogeneous and heterogeneous systems are divided into fog, smoke, aerosol, emulsion, suspension, foam, etc., as shown in Tab. 1.

Dispersion medium	Dispersed phase	Disperse system	
		colloidal	coarse
gas	gas	-	-
	liquid	aerosols (e.g. fog)	rain, fogs
	solid	aerosols (e.g. smoke)	dust, smokes
liquid	gas	foams	bubbles, foams
	liquid	emulsions	emulsions
	solid	lyosols	suspensions
solid	gas	solid foams	solid foams or e.g. minerals with gas inside
	liquid	solid emulsions (gels)	solid emulsions or e. g. minerals with droplets inside
	solid	solid salts	solid compounds (e.g. alloys)

Table 1: Classification of heterogeneous and homogeneous systems [2]

- according to shape of the particles of the disperse phase
  - globular systems – particles have a globular shape (isometric particles)
  - laminar systems – one dimension of particles is significantly smaller than the others (anisometric particles)
  - fibrillar systems – one dimension of particles is significantly greater than the others (anisometric particles)
- according to a size distribution of the particles
  - monodisperse systems – consist of particles all of nearly the same size
  - paucidisperse systems – consist of particles of only a few sizes
  - polydisperse systems – consist of particles of many different sizes

There are also many other ways of dividing disperse system but they are not important.

2.1 Aerosols

In Tab. 1, there is shown that aerosol is a collection of solid or liquid particles dispersed in gas. The stability of dispersed particles can vary from a few seconds to years. Aerosols are everywhere around us. They can originate naturally (e.g. clouds) as well as the result of humankind activities (e.g. pollutant particles in the atmosphere or some medical application). In both cases, it is important to know the composition of aerosols. This knowledge enables us to better understand nature phenomena for example. In many humankind activities, the knowledge of aerosol composition is nearly crucial. In energy technology, it is possible to reduce the harmful impact of products created during the combustion process for example. [1], [4]

We can say that aerosols are two-phase systems. Such two-phase systems have different properties depending on sizes of particles and also their concentration in the dispersion medium. The particulate phase of aerosols usually represents only a small friction of its total mass and volume – less than 0,0001%. Therefore, bulk properties of aerosols (e.g. density, viscosity) differ imperceptibly from those of pure air. Consequently, we must apply the microscopic point of view in order to study aerosols properties. It means consider one particle at time and deal with the forces on the particle, its motion, interaction with the dispersion gas, with other particles etc. [1]

Most aerosols are polydisperse systems. In order to characterize these systems, some statistical measurement needs to be done.

2.2 Properties of polydisperse systems

The most important property for characterizing the behaviour of polydisperse systems is particle size. All properties of the system depend on the size of particles. That is the reason for applying the microscopic approach and characterizing the properties on an individual

particle basis. After that, average properties can be estimated by integrating over the size distribution. [1]

Another property that influence the behaviour of polydisperse systems is a shape of dispersed particles. It is usually assumed that the particles are spherical, which is not always true. Therefore, the correction factors and equivalent diameters are used. An equivalent diameter is a diameter of an imaginary spherical particle, that has the same value of the particular property as the original nonspherical particle. [1], [4]

The particle density is also the property of interest. It is important to bear in mind that it is the density of the particle itself, not the density of the system. Liquid and crushed solid particles have the same density as their parent material. The density can be often gained by simply measurement (e.g. using pycnometer). [1]

The mass concentration is the most commonly measured property of such systems. In contradistinction to the three properties mentioned above, this is not a property of particles but of the whole system. The mass concentration is the total mass of particles in a unit volume of the polydisperse system. Common units are g/m^3, mg/m^3 or $\mu g/m^3$. [1], [4]

The mass concentration is not the only concentration that can be measured. The number concentration gives us the number of particles in a unit volume of the system. It is usually expressed as $number/m^3$ or $number/cm^3$. [1], [4]

2.3 Analysis of polydisperse systems

The only parameter is needed to characterize the particle size of monodisperse systems and it is the particle diameter. However, as mentioned earlier polydisperse systems are collections of particles distributed in the dispersion medium where each particle has a different size than the others. The particle sizes can range over two or more orders of magnitude. Because of this wide size range and the fact that the properties of polydisperse systems strongly depend on particle sizes, it is necessary to characterize the size distribution by statistical means. [1], [4]

2.3.1 Determination of system distribution

Although analysis results of a polydisperse system sample can be kept completely, in most cases it is not convenient. Firstly, the large amount of data has to be stored, and secondly, it is an awkward format for other processes, from which we would like to gain several different kinds of statistics that describe the properties of polydisperse systems. For these statistics, it is necessary to know how the particles are distributed among the various sizes. [1]

In order to get a particle distribution, it is needed to divide the entire size range into a several particle size intervals and determine the number of particles in each interval. The

intervals must be contiguous so that the size upper limit of each interval coincides with the lower limit of the next higher interval. The intervals must also cover the entire size range. [1]

Such data can be represented in many graphical ways. One of them is the histogram, an example is shown in Fig. 1, where the width of each column represent the size interval and the height represents the number of particles in the particular interval. [1]

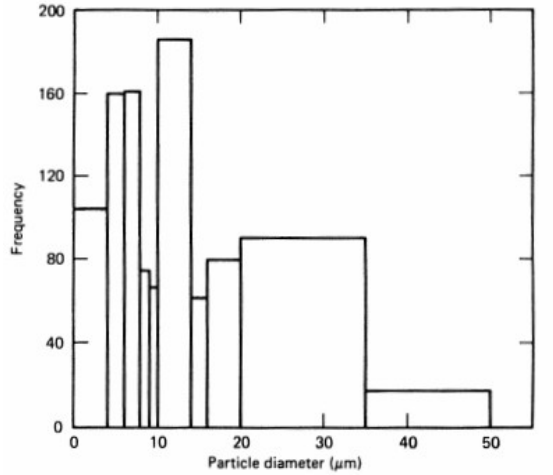

Figure 1: The histogram of the particle distribution [1]

From Fig. 1, it is obvious that such a representation provides a distorted information because the height of any columns depends on the width of the interval. In larger interval, there is naturally more particles than in the smaller one. In order to prevent this fact, the histogram is normalized for interval width by dividing the number of particle in each interval by the width of that interval. The height of each column is then expressed as the number of particles per unit of size interval – e. g. number/μm, as shown in Fig. 2. [1]

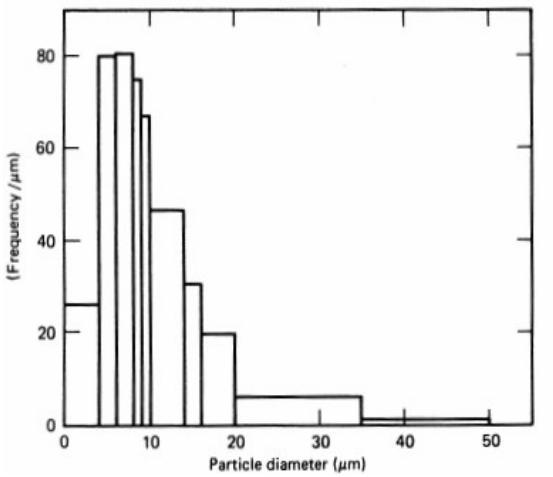

Figure 2: The normalized histogram of the particle distribution [1]

After this adjustment, heights of columns with different widths are comparable. Furthermore, the area of the column is proportional to the number of particles in the size interval. Consequently, the total area of all columns is the total number of particles in the sample, mathematically expressed in Eq. 1.

$$N = \sum_i h_i \cdot \Delta d_i \ , \qquad (1)$$

where N is the total number of particles, h_i is the height of the column and Δd_i is the width of the column. [1]

The histogram is also usually standardized for the particular sample by dividing the height of each column by the total number of particles in the sample. After that, heights are given as fraction per unit of size interval, e.g. fraction/μm, as shown in Fig. 3. [1]

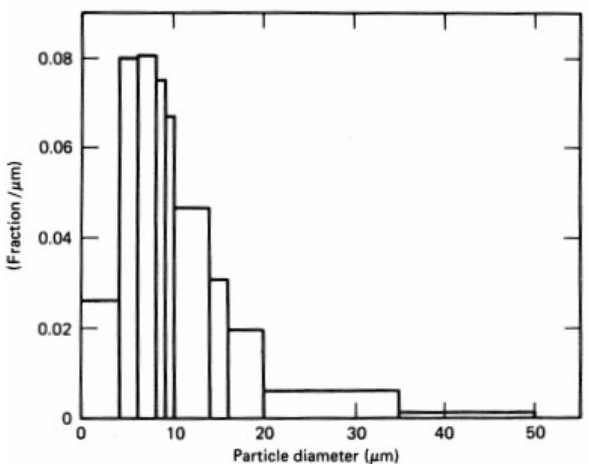

Figure 3: The histogram of particle distribution after the standardization for the sample [1]

Both the distribution in Fig. 2 and in Fig. 3 have the same shape. The only difference is the unit of the ordinate y, where the unit of fraction/μm is in Fig. 3.

The area of the column after the standardization equals to the fraction f_i of particles in the size range and the total area $\sum_i f_i$, which is shown Eq. 2, is equal to 1. [1]

$$\sum_i f_i = \sum_i h_i \cdot \Delta d_i \qquad (2)$$

This standardization allows the direct comparison of histograms obtained from different samples.

When all these processes are done, we can obtain a smooth curve of the particle distribution, as in Fig. 4, by using many small columns and drawing the curve through their tops. [1]

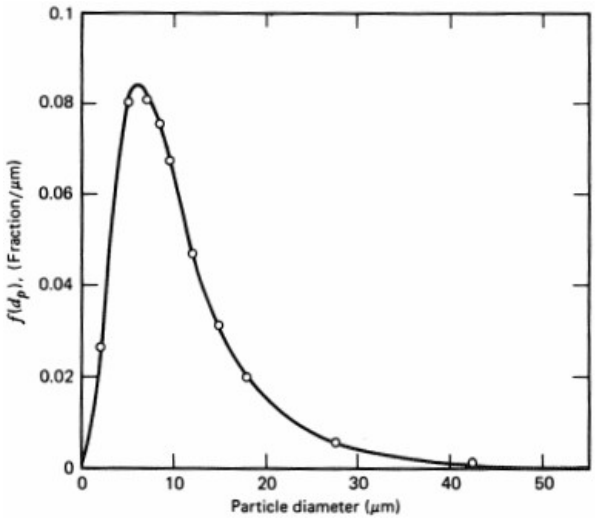

Figure 4: The particle distribution curve [1]

Such a curve is the graphical representation of the frequency function, or probability density function, and is useful for mathematical interpretation. The fraction of the total number of particles *df* having diameters between d_p and d_p+dd_p is $df=f(d_p)dd_p$, where $f(d_p)$ is the frequency function and dd_p is the differential interval of particle size. By integrating the frequency function between two sizes *a* and *b* in Eq. 3, the area under the curve is obtained, which equals the fraction of particles whose diameter fall within this interval. [1]

$$f_{ab}=\int_a^b f(d_p)dd_p \qquad (3)$$

Size distribution can also be presented as cumulative and complementary cumulative distribution function. The cumulative distribution function, an example is in Fig. 5, is defined by Eq. 4 and it gives the fraction of particles having diameter less than *a*. [1], [5]

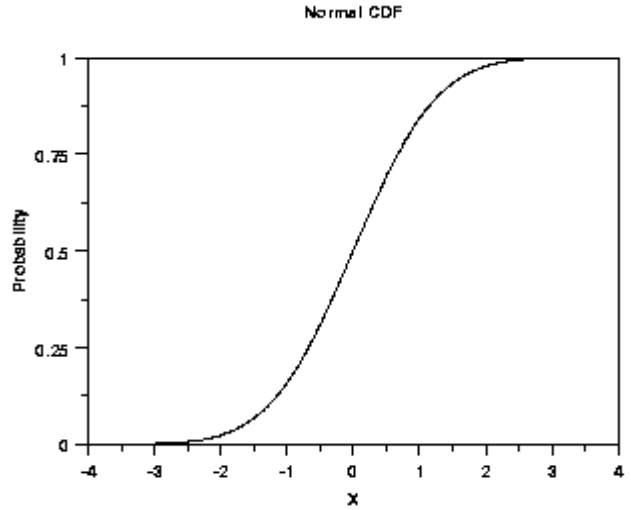

Figure 5: Example of a cumulative distribution function [5]

$$F(a)=\int_0^a f(d_p)\,dd_p \tag{4}$$

On the contrary, the complementary cumulative function $S(a)$, of which example is in Fig. 6, describes the fraction of particles having diameter greater than *a*. [5]

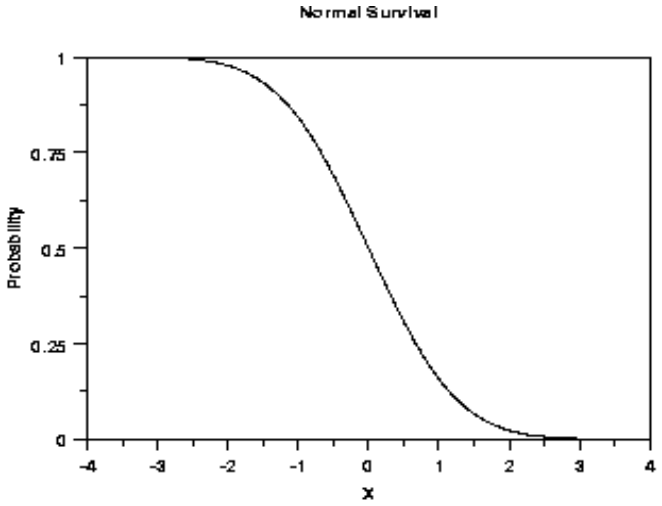

Figure 6: Example of complementary cumulative distribution function [5]

The relationship between these functions is mentioned in Eq. 5. [5]

$$F(a)+S(a)=1 \tag{5}$$

These cumulative and complementary cumulative distribution functions make possible to determine readily the quantitative information about the particle distribution. In the case of the former, the fraction less than the given size, and in the case of the latter, the fraction greater than the given size can be read directly from the graph. The fraction of particles having diameters between sizes *a* and *b* can be found according to Eq. 6 by simple subtracting the cumulative function for size *a* from that for size *b.* [1]

$$f_{ab}=F(b)-F(a) \tag{6}$$

If the complementary cumulative function is needed to be used, the term in Eq. 7 gives the same result. [1]

$$f_{ab} = 1 - [S(a) - S(b)] \quad (7)$$

2.3.2 Mathematical models

During the analysis, the number of particles in the particular range is obtained at first. In order to acquire the distribution curves, the mathematical distributions are applied. The most common distributions utilized in particle size analysis are Rosin-Rammler and log-normal distributions. Each distribution is suitable for a slightly different system of particles, however, in many cases only an experiment determine which distribution suits more.

2.3.2.1 Rosin-Rammler distribution

The Rosin-Rammler distribution is usually applied on systems that has a wide range of irregular particles, such as moon dust, crushed coal, or even droplets of liquid sprays. It is very useful for determination of the distribution after the sieves analysis or for distribution that are more skewed (longer tail at large particle diameters) than log-normal distribution. The frequency function of the Rosin-Rammler distribution is shown in Eq. 8.

$$f_{RR}(d_p) = \alpha \cdot n \cdot d_p^{n-1} \cdot \exp(-\alpha \cdot d_p^n), \quad (8)$$

where d_p is the particle diameter, α and n are constants. Constant α depends on the fineness of particles and constant n depends only on their material. The example of values for constants α and n for some materials is given in Tab. 2. [1], [6]

material		α	$n \cdot 10^3$ [1/μm]
fine grinding	marlstone	0,675	33
	brown coal	0,900	63
	glass powder	1,111	25
coarse grinding	coal	0,781	0,15
	limestone	0,933	0,083
	clinker	1,036	0,50

Table 2: Examples of values for α and n [6]

Integrating the frequency function yields cumulative distribution function shown in Eq. 9. [6]

$$F_{RR}(d_p) = 1 - \exp(-\alpha \cdot d_p^n) \quad (9)$$

Finally, the complementary cumulative distribution function is shown in Eq. 10. [6]

$$S_{RR}(d_p) = \exp(-\alpha \cdot d_p^n) \quad (10)$$

The latter can be also expressed as Eq. 11. [6]

$$\ln\left(\ln\frac{1}{S_{RR}}\right)=\ln n+\alpha\cdot\ln d_p \qquad (11)$$

Using log-log coordinates, the term $\ln\left(\ln\frac{1}{S_{RR}}\right)$ versus $\ln d_p$ provides a linear dependence. From the slope and the point of intersection of this straight line, α and *n* can be determined, respectively. In practise, two values of S_{RR} and d_p from the analysis are used for obtaining the straight line. [6]

2.3.2.2 *Log-normal distribution*

The log-normal distribution is suitable for systems of fine particles where the ratio of largest to the smallest particles is recommended to be greater than 10. Unlike the normal distribution, the log-normal distribution is not symmetrical and thus it is possible to utilize it as approximation for, in most cases, skewed distribution of particles. [1], [6]

The frequency function of log-normal distribution is shown in Eq. 12. [1]

$$f_{\ln}(d_p)=\frac{1}{\sqrt{2\cdot\pi}\cdot\ln\sigma_g\cdot d_p}\cdot\exp\left[-\frac{(\ln d_p-\ln d_{[0,1]})^2}{2\cdot(\ln\sigma_g)^2}\right], \qquad (12)$$

where σ_g is the geometric standard deviation and $d_{[0,1]}$ is the number median diameter. The geometric standard deviation is defined by Eq. 13.

$$\ln\sigma_g=\left(\frac{\sum_i n_i(\ln d_i-\ln d_g)^2}{N-1}\right)^{1/2}, \qquad (13)$$

where n_i is the number of particles in group i having a midpoint d_i, d_g is the geometric mean diameter and N is the total number of particles. [1]

The cumulative distribution function could be obtained, following Eq. 4, by integrating the frequency function.

There are also many other distributions that might be used, such as Weibull, exponential, or Nukiyama-Tanasawa distribution, that are applied in special situations. For example, exponential distribution was successfully utilized analysing powdered materials. All distributions, including Rosin-Rammler and log-normal distribution, have been chosen empirically in order to obtain the best approximation of the system distribution. [1]

2.3.3 Determination of the particle diameter

As was mentioned earlier, particles in polydisperse systems are usually not regular-shaped objects and thus we cannot easily work with a single dimension that represents them. The only object that can be described by one unique dimension is the sphere. Nevertheless, even a particle can be described by many unique numbers concerning various properties of

the particle, for example, weight, volume or surface area. After that, the unique number value (e.g. weight) of the particle can be converted into the diameter of the imaginary sphere that has the same value of the unique number (e.g. weight) as the measured particle. This technique is called the equivalent sphere theory. Due to this theory, three dimensions are not needed to describe 3D particles, which would be more accurate but very inconvenient for other processing, too. [1], [7]

There are also some obstacles that have to be born in mind when using the equivalent sphere theory. The unique number that is used needs to be chosen carefully in order to obtain appropriate results. For example, when we look at the particles under the microscope, we are looking at some 2D projection and we can measure a number of diameters to characterise the particle. Obviously, if we take the maximum length of the particle, the results differ to the contrary case when we take the minimum length. Hence, it is important to remember that each measuring technique uses a different property of the particle and therefore the results of various techniques differ, as indicated in Fig. 7. [7]

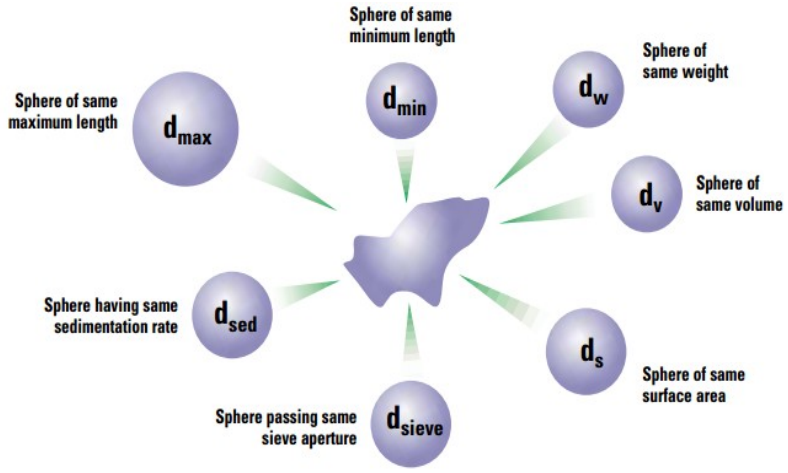

Figure 7: Example of different results for different techniques [7]

The simplest approach to obtain one average particle diameter from a large amount of data is the ordinary arithmetic average. In Eq. 14, one can see that it is the sum of all particle sizes divided by the number of particles. [1]

$$d_{[1,0]} = \frac{\sum n_i \cdot d_i}{\sum n_i} \quad , \tag{14}$$

where n_i is the number of particles in group i having a midpoint d_i and the summations are over all intervals. [1]

This is a number length mean. The word number is in the name because the number of particles appears in the equation. In mathematical terms, it is called the $d_{[1,0]}$ because the diameter terms on the top of the equation are to the power of (d^1) and there are no diameter terms (d^0) on the bottom. [1], [7]

Another characterizing particle diameter is based on considering the surface area. The surface area is a function of the diameter squared therefore Eq. 15 is valid. [1]

$$d_{[2,0]}=\sqrt{\frac{\sum n_i \cdot d_i^2}{\sum n_i}} \tag{15}$$

This is a number surface mean because the number of particles appears on the bottom of the equation. There is the summation of the diameters squared in the equation so in mathematical terms this is called the $d_{[2,0]}$ – diameter terms squared on the top, no diameter terms on the bottom. [7]

In some cases, it can be useful to find the diameter considering the weight or the volume. The volume is gained using the third power of the diameter and thus Eq. 16 is used to obtain the mean diameter. [1]

$$d_{[3,0]}=\sqrt[3]{\frac{\sum n_i \cdot d_i^3}{\sum n_i}} \tag{16}$$

This is a number-volume or number-weight mean. Number of particles again appears in the equation therefore this is also a sort of number mean. In mathematical terms, this can be seen as $d_{[3,0]}$. [7]

All preceding means have one significant drawback which is the necessity to know the total number of particles. Particle counting is usually carried out only in applications when the numbers are very low (ppm concentrations), such as contamination, control and cleanliness. [7]

Hence, so called moment means are introduced. The count or number distribution are not the only distributions that can be used. Another distributions are the surface area (also known as the second-moment) distribution and the mass (the third-moment) distribution. While the number distribution gives the fraction of the total number of particles in any size range, the mass distribution gives the fraction of the total mass of particles contributed by particles in any size range. Analogous statement could be written about the surface area distribution. The moment distributions can be drawn in the graph, too. The graphical representations differ from each other and thus respective mean diameters are also different. [1]

The surface area mean diameter can be written in form analogous to number length mean, as shown in Eq. 17. [1]

$$d_{[3,2]}=\frac{\sum s_i \cdot d_i}{\sum s_i}=\frac{4\pi \sum n_i \cdot d_i^2 \cdot d_i}{4\pi \sum n_i \cdot d_i^2}=\frac{\sum n_i \cdot d_i^3}{\sum n_i \cdot d_i^2}\ , \tag{17}$$

where s_i is the surface of all particles in a group i with a midpoint d_i. This mean diameter is also called the Sauter diameter.

Since Eq. 18 and Eq. 19 are valid, the Sauter diameter can be written in the form of Eq. 20. [1]

$$\sum n_i \cdot d_i^3 = N \cdot d_{\bar{m}}^3 \ , \tag{18}$$

where N is the total number of all particles and $d_{\bar{m}}$ is the diameter of average mass.

$$\sum n_i \cdot d_i^2 = N \cdot d_{\bar{s}}^2 \ , \tag{19}$$

where $d_{\bar{s}}$ is the diameter of average surface.

$$d_{[3,2]} = \frac{d_{\bar{m}}^3}{d_{\bar{s}}^2} \tag{20}$$

In the similar fashion the mass mean diameter then follows Eq. 21. [1]

$$d_{[4,3]} = \frac{\sum m_i \cdot d_i}{\sum m_i} = \frac{\pi \cdot \rho_p / 6 \sum n_i \cdot d_i^3 \cdot d_i}{\pi \cdot \rho_p / 6 \sum n_i \cdot d_i^3} = \frac{\sum n_i \cdot d_i^4}{\sum n_i \cdot d_i^3} \ , \tag{21}$$

where m_i is the mass of all particles in a group i with a midpoint d_i and ρ_p is the density of particles. This kind of mean diameter is also called the De Brouckere mean diameter and it can be written also in the fashion of Eq. 22. [1], [7]

$$d_{[4,3]} = \frac{d_{\bar{c}}^4}{d_{\bar{m}}^3} \tag{22}$$

The latter two means represent, in analogy to the moment of inertia in classical mechanics, the centre of gravity of the surface area and mass distribution, respectively. The advantage of these means is obvious – the formulae do not contain the numbers of particles and therefore in the calculations there is not required the knowledge of the number of all particles. [7]

Although each calculation technique gives different results, none of them is wrong. All techniques are right because each considers different property of the particle. Thus, we can compare only results obtained by the same technique. Consequently, there cannot be anything like particle size standard for particles, such as grain of sand, for mutual comparison of techniques. There must be a spherical standard in this case. However, there can be set up a particle size standard for a particular technique, which allows to compare results of the instruments that use this technique. [7]

Application of particular mean diameter depends on a different kind of factors. One of the most important factor is the measuring method of particles. Some of them provide only a partial piece of information about the particle dimensions thus only the simplest mean diameter can be calculated. For example, electron microscope provides the 2D image, from which we can easily calculate diameter $d_{[1,0]}$ but obtain Sauter diameter from this image is not possible. Another key factors are the composition of the analysed system and the subsequent utilization of the diameter. [7]

2.3.4 Basic statistical evaluation – mean, median, mode

The most commonly used statistical quantities used in the evaluation process of particle size analysis are the mean, mode and median. In general, these and several other quantities are included in the term averages. [1]

The mean is also called arithmetic average and it is simply the sum of all processing values divided by the number of the values. There is a number of means that can be calculated for particle sizes and they were discussed in detail in previous text. [7]

The median is the value which divides the distribution exactly in two equal halves therefore one half of the total number is smaller than the median value and the other half is larger. That means that median also divides the frequency distribution curve into two equal areas. [7]

The mode is the most frequent value in the statistical set. In other words, it is the highest point of the frequency distribution curve. [7]

For symmetrical distributions, e.g. the normal distribution in Fig. 8, the mean, median and mode is exactly the same value, which corresponds to the axis of symmetry. [1]

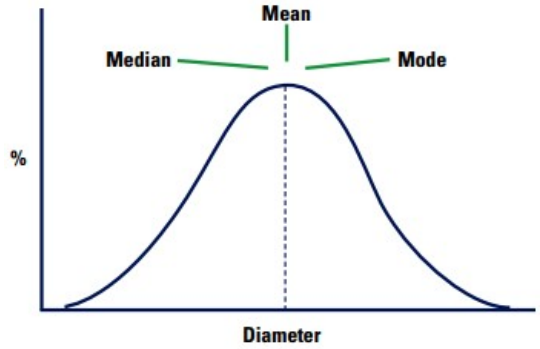

Figure 8: The symmetrical distribution [6]

However, for the asymmetrical distribution in Fig. 9 the values for the mean, median and mode are different.

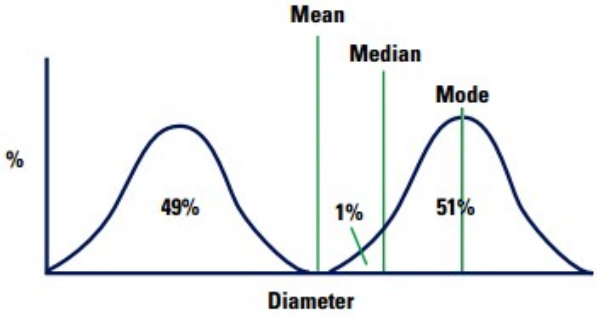

Figure 9: The asymmetrical distribution [6]

The mean is almost exactly between the two peaks of the distribution while the median lies 1% into the larger part of the distribution because this is the point that divides the whole

distribution into two halves. The mode is situated in the middle of the larger part of the distribution since this is the most common value throughout the distribution. [7]

3 Examples of measuring methods

There is a huge number of various instruments used in order to obtain the particle size distribution. Commercially available instruments can be used as well as a special designed instrument for a very specific application. Some of these instruments can be used in on-line mode of operation. These are integrated into the manufacturing process and work while the process is under way. There are also instruments for off-line mode of operation. Most instruments carry out the analysis in batches, nevertheless there are also some instruments that work in the continuous way. Instruments can be used for analysing dry set of particles or particles dispersed in some kind of suspension. The analyse should be carry out in the disperse system similar to that in which the particle set will be used. [8]

The choice of the suitable instrument is affected by many factors. First of all, the properties of the analysed polydisperse system, such as composition or estimated particle size range must be considered. It is also important to take into account the amount of sample available, the way of interpretation of acquired data, cost of instruments etc. [8]

The particular instrument uses the specific measuring method and thus the choice of the instrument determined also the method. As was mentioned earlier, results obtained from different methods cannot be usually compared. Therefore, particle size measurements are often considered as relative measurements and results from one analysis can be compared only with those obtained on the same instrument in the similar conditions. [8]

3.1 Sampling of the system of particles

For the analysis of the system, which is usually a huge bulk, only a fraction of it is needed. Naturally, the first step in the analysis procedure is the reliable and precise sampling process. The goal is to collect a small amount of the polydisperse system from the bulk quantity which represents very well physical and chemical properties of the entire bulk. [8], [9]

There are specific recommendations for the sampling process summarized in three basic rules [9]:

- particles of the systems should be in motion
- the sample should be taken from the whole stream of particles in many short increments of time (should not be taken from parts of the stream for the whole time)
- the entire bulk of the polydisperse system should pass through the sampling device

The sampling process can be supplemented with mathematical techniques. It reduces amount of time and effort spent in sampling because the examination of only fraction of the bulk is sufficient. The mathematical techniques also provide the possibility of calculating the level of uncertainty. [8]

3.2 Sieving

Sieving is one of the oldest method used in analyses of polydisperse systems. The principle is simple. The sieve retains the larger sized particles than a design aperture size and allows smaller particles to go through. The basis of this method is a set of such sieves with different opening size placed in decreasing order under each other so that the sieve with the largest aperture is on the top. Sieves are usually driven in order to shake and thus the sample goes through the sieves more easily. The sieve analysis is suitable for systems with particle sizes in the range from approximately 125 mm to 20 μm and sieves are classified as coarse (100 – 4 mm aperture size), medium (4 mm – 200 μm), and fine (less than 200 μm). After the passing through sieves, the samples are weighted and subsequently the weight distribution can be carry out. [8]

In general, sieving techniques can be divided in two categories, namely dry sieving and wet sieving. Dry sieving is to a large extent still carry out by hand, nevertheless some steps for automation, that should provide better efficiency and minimize errors during process, have been done. The basic improvement is an automatic vibratory motion of the sieves, which helps particles to go through and reduce the sieving time. Wet sieving is carried out in cases when the analysed system consists of a very fine particles (typically smaller than 50 μm) that tend to agglomerate. The sample is converted into suspension that passes all levels of sieves. After that, the samples from particular sieves are dried out and can be analysed. [8], [10]

Although it is one of the oldest methods, it is still extensively used. The main advantages are simplicity, low investments and operation costs, high reliability and relatively low technical expertise required for performing. Disadvantages are the difficult analysis of systems with particles smaller than 20 μm or agglomerated materials, and a possible distortion of the distribution if the measurement is carried out for too long. Therefore, measurement times are standardised. [7], [8]

3.3 Sedimentation

Sedimentation method is one of the most common methods used in analysis of polydisperse systems. It utilizes the gravitational force acting on the particles dispersed in the fluid. The gravitational force has to overcome the buoyancy in the fluid and other drag forces. The principle is the measurement of the velocity of the descending particles. This relationship is described by Eq. 23, that is known as Stokes' law.

$$v = \frac{d_p^2 \cdot (\rho_p - \rho_f) \cdot g}{18 \cdot \eta_f} \quad , \tag{23}$$

where v is a settling velocity of the particle, d is the particle diameter, ρ_p and ρ_f are the particle and fluid densities, respectively, g is gravitational acceleration, and η_f is the viscosity of the fluid. [8]

Stokes' law is valid only for laminar flow and particles unaffected by Brownian motion. Therefore, the sedimentation is suitable for particle size in the range 50 – 2 μm. Particles larger than 50 μm can cause turbulent flow in many fluids, on the contrary, movement of smaller particles than 2 μm is influenced by Brownian motion. [11]

Sedimentation can provide sufficient results only for systems consisting of particles with the same density. It is important to know the density of particles that have to differ adequately from the density of the fluid. The difference can be adjusted by choosing a suitable fluid, however, the conditions of the laminar flow must be met. The temperature of the fluid must be controlled very accurately, otherwise the viscosity changes and thus the sedimentation process is affected. [7], [8]

In practise, the concentration of particles at different depths in the fluid is measured. There are two methods measuring the concentration. X-ray sedimentation and photo-sedimentation methods utilize x-rays and light beams, respectively. Both methods work on the principle of intensity attenuation of the beam. In the case of x-ray beam, the attenuation is caused by absorption while light beam is attenuated due to scattering. The intensity after the attenuation is compared with initial intensity of the beam. After obtaining the concentration at various depths, the settling velocity of particles can be determined. [8]

Since the settling time can be very long, especially for very fine particles, an external centrifugal force is sometimes added. The sample is injected in centre of rotating disk and due to centrifugal force the separation takes place. Centrifugal force minimizes the effect of Brownian motion and drag forces and thus instruments equipped with centrifugal capability are reliable even for particles smaller than 2 μm. [8], [11]

The acquired diameter is so called Stokes diameter and represents the diameter of sphere that would settle with the same velocity as the real particle. [7]

3.4 Laser diffraction

The laser diffraction method is correctly called low angle laser light scattering (LALLS). This method utilizes the interaction between a laser beam and a surface of particles. Laser light incident on a particle is diffracted producing a scattered light pattern which is captured by detectors around the volume of the sample of particles. Diffraction is a phenomenon occurring at any obstacle of comparable size to the wavelength of the wave encountering the obstacle. Concerning the laser diffraction method, small differences in the path length of light waves created upon interaction with particles cause constructive and

destructive interference of scattered light waves and it leads to characteristic diffraction patterns. The direction of scattered wave depends on the particle shape and size. [7], [8]

Instruments using this method comprise of three main components, that are a source of light (typically He-Ne gas laser with the wavelength of 0,63 μm), a sample cell within the analysed sample is introduced, and detectors (optical elements) that convert the scattered light intensity into the electrical signal which is then processed to obtain the particle size distribution. A schematic diagram of such an instrument is shown in Fig. 10. Some instruments are equipped witch other accessories to prevent particles in the sample from agglomeration, which is an important factor for reliability of the measurement. Agitators or pumps for keeping the sample circulating can be used. [7], [8]

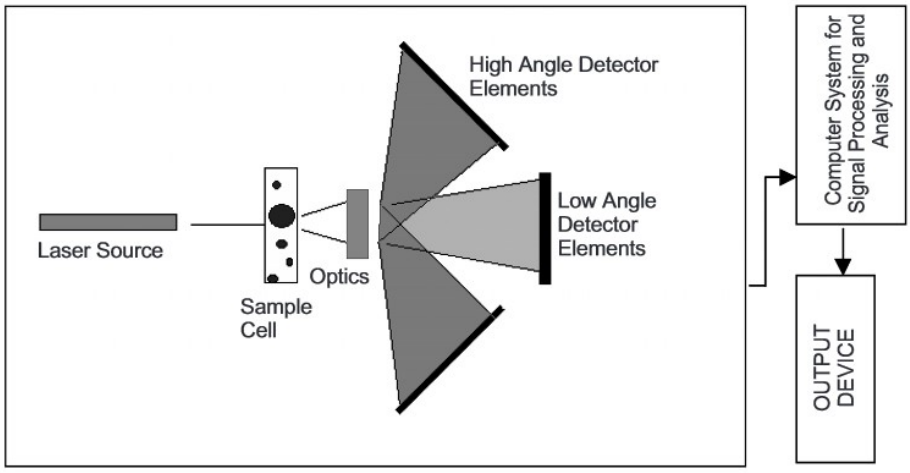

Figure 10: A schematic diagram of a laser diffraction instrument [8]

There are three basic assumption in laser diffraction. Firstly, particles are considered to be spherical. Secondly, the once scattered light does not interact with another particle and gets scattered again, i.e. there is no multiple scattering. In order to meet this assumption, the concentration of particles in the sample is limited. Thirdly, the light pattern captured at the detectors is the sum of individual patterns generated by each particle interacting with the laser beam. [8], [11]

Laser diffraction instruments can be used for analysing both dry powders and liquid suspensions. Usually, the sample is investigated off-line, though there are some special designed instruments that allow performing the analysis from a moving stream on the on-line basis. Regarding off-line measurement, the entire sample is measured and thus the ultimate distribution is acquired from all particles. On the contrary, the sample is usually very small (one or two grams) and must be representative. This method is rapid and highly repeatable. [7], [8]

3.5 Microscopy

Compared to other methods of particle size analyses, microscopy-based techniques provide a possibility to examine the particle shape in addition to the measurement of size. These

techniques are very illustrative as they allow to directly see the particles in question. Consequently, the image is evaluated and the particle size is determined based on a defined measure of diameter. Data are usually expressed as diameter of a sphere that has the same projected area as the actual projected particle. [7], [8]

Microscopy-based techniques enable to study various materials with broad range of particle sizes, from millimetres to nanometres. Conventionally used instruments include optical light microscope, scanning electron microscope or transmission electron microscope. The choice of the instrument is dictated by the size range of particles, desired magnification and resolution. Naturally, the costs rise as higher magnification, resolution and reliability are required. Optical light microscopes are cheaper and easier to operate and maintain but they are more limited in magnification and resolution in comparison to electron microscopes. With careful selection of the objective, the particle size limit is close to one μm. Scanning electron microscope is suitable for particle size range of 1000 – 0,1 μm and transmission electron microscope enables analyses in the size range of 10 – 0,01 μm. In Fig. 11, there is shown the relationship between the investigated particle size and the instrument suitable for the analysis. [8], [12]

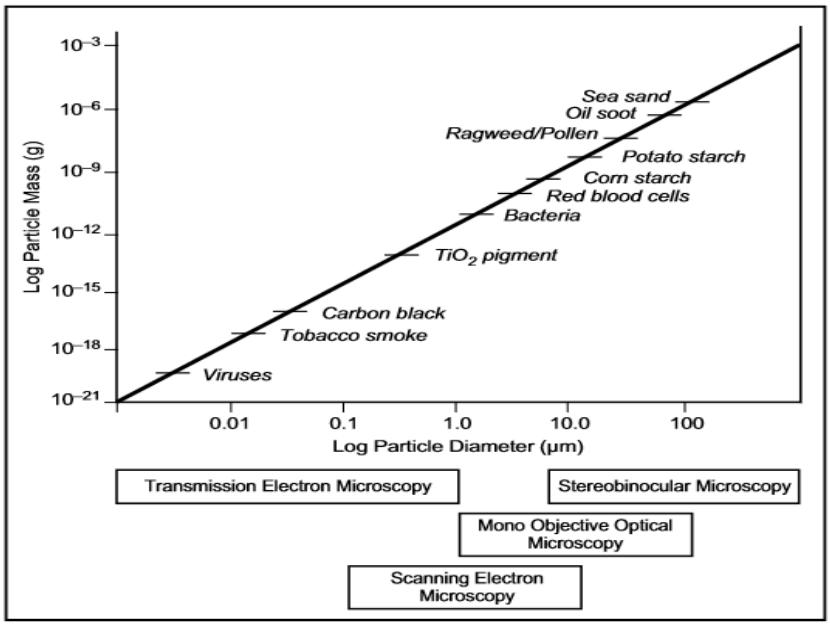

Figure 11: The relationship between particle sizes and instruments suitable for analysis [8]

The difficulty of sample preparation for analysis by microscope-based techniques depends also on the microscope type. The sample preparation for optical microscopes is relatively easy and can be done in a short period of time. On the contrary, the transmission electron microscope requires greatest amount of effort and time for the proper preparation of the sample. Both electron microscopes has a significant advantage related to depth of focus that enables observing of particles of different sizes simultaneously without refocusing on each particle. In other words, even particles of significantly different sizes are viewed in

the same field of focus. Optical microscopes have limited depth of focus and thus the refocusing is often necessary. [8]
Since relatively few particles are examined, the sample must be truly representative. This statement is valid for all techniques, however, it is even more important when the particle size gets smaller. Special attention must be paid for systems with broad range of particle sizes and for systems that tends to agglomerate. This means that particles should be well dispersed in the system before the sample is taken, and the number of particles touching each other in the sample should be minimized, and should be proportional to that which appears in the whole system. Particles can be examined in dry state as well as in suspensions. The number of particles needed to be analysed, in order to get results with sufficiently low statistical errors, is given by standards. [7], [8]

The analysis itself can be performed manually, semi-automatically or automatically. During the manual analysis, the particle sizes are determined using a marking device such as a cross-hair that moves along to the particle to obtain a characteristic linear dimension, or graticule that has inscribed circles of different sizes that are compared with projected particles. The semi-automated techniques require human interventions as well but have some degree of automation. The typical example of semi-automated technique is the analysis utilizing the digitalized image of particles when the area of particles is calculated. Before the evaluation, the image is adjusted (e.g. converted into a gray-scale image) so that the particles are more evident and results more precise. During automated techniques, the captured image is interpreted using special algorithms. The most significant advantage of automated techniques is the reduction of time required for the analysis. On the other hand, the operator interventions are limited, which can lead to an analysis of unwanted features or analysis with inappropriate parameters. However, most modern systems usually allow adjustments by the operator. [8]

3.6 Photogrammetry

The last two categories, namely semi-automated and automated techniques that utilize recorded images for evaluation of the particle sizes could be classified as part of the photogrammetry. Photogrammetry is the science that uses photographs for measuring shapes and positions of projected objects as well as distances between them. The output of photogrammetry methods can be a map, drawing, measurement or specific 2D or 3D model of projected objects, for example. It is used in various fields, such as topographic mapping, geology, architecture, mechanical engineering, or quality control. [13], [14]

In general, photogrammetry can be divided in many categories following different criteria. Depending on the recorded range, photogrammetry can be arrange in three categories [15]:

- space photogrammetry
  In this case, photographs are taken by space vehicles and whole planets and their surfaces are recorded and subsequently examined.
- aerial photogrammetry
  Photographs are taken by airplanes, helicopters or balloons. The goal is to record Earth's surface, which can be useful for creating maps, for example. Taken pictures can be either single (orientational) or composites of overlapping photographs.
- close-ranged photogrammetry
  Photographs are taken by cameras attached to tripods in a steady position. Smaller objects such quarries, mines, buildings, engineering structures or human bodies are recorded.

According to a way of photograph evaluation, three categories are established [13]:

- single-image photogrammetry
  Single photographs are evaluated and the output is a plane image. Thus, the knowledge of one dimension is missing and it leads to a lower accuracy and only limited application.
- double-image photogrammetry (stereophotogrammetry)
  The output is a 3D model since two photographs of the same object (area) taken from two different places are processed.
- multi-image photogrammetry
  More than two photographs are processed therefore the final model is very accurate. This method made a significant progress due to the progress in computer and software technology and thus it is a versatile and rapid method nowadays.

Naturally, the development of photogrammetry depends on the development of science and technology and thus, from the historical point of view, photogrammetry is divided in four generations [15]:

- first generation (approx. 1850 – 1900)
  The first generation started shortly after the invention of photography. It was mainly experimental phase, nevertheless a significant progress in terrestrial and balloon photogrammetry was achieved.
- analog photogrammetry (approx. from 1900)
  The second stage started with the invention of the stereophotogrammetry in 1901. Instruments were based on mechanical and optical principles. After the inventions of the airplane, the fundamentals of aerial photogrammetry were established and they are valid until today.

- analytical photogrammetry (approx. from 1950)
  The third generation started with the advent of computers, which made numerical solutions possible. As a consequence, the accuracy was improved considerably.
- digital photogrammetry (approx. from 2000)
  The latest generation utilizes digital images that can be taken directly or the former photographs can be digitalized. Analytical methods are usually used for processing the image in digital photogrammetry.

Very important part of photogrammetry that affects the result of the whole process is data acquisition. The reliable information about surfaces and properties of the recorded object is needed, moreover, this information is obtained without a direct contact with the object. The device for data acquisition is called sensor and the most typical representative is a camera. Nevertheless, the image can be acquired using different device as well, for example, microscopes, scanners, or camcorders. [14], [15]

After that, the photograph is processed so that the intended piece of information is obtained. Photographs in the form of digital images are adjusted in order to make the analysis possible and accurate. This adjustment consists of transformations, determination of orientations, digital rectification, edge detection etc. Eventually, the required measurements can be carried out and visualisation can be done, for example. [13], [15]

4 Measurements in steam turbines

4.1 Wet steam in steam turbines

During the expansion process in a steam turbine, the composition of the working fluid changes. The initial dry steam transforms into the wet steam due to the change of the pressure and temperature. The last part of the turbine, the low pressure stage, is affected by the presence of the water fraction in the steam. Wet steam as a working fluid brings several disadvantages in the process. Firstly, wet steam in the low pressure stage decreases the power and efficiency of the turbine due to complicated irreversible processes. Secondly, water droplets cause erosion of the blades, which can lead to the blade failure. This increases demands for the maintenance and decreases lifetime. That is the reason why studies of the wet steam in the low pressure stages are needed.

Four phases occur in the wet steam formation and evolution during the expansion [16]:

- steam
- condensation fog (fine droplets)
- water rivulets on blades and inner casing
- coarse droplets

Dry steam at high pressure and temperature enters the turbine high pressure stage. As the expansion is under way, the pressure and temperature decrease and first water droplets form. These droplets are very small (0,2 – 1 μm in diameter) and does not significantly influence the turbine power nor its blades. Condensation fog consists of such fine droplets. In low pressure stages, the overall wetness of the steam increases and the droplets start to form water films and subsequently rivulets on stator blades and inner casing. The rivulets disrupt at trailing edges of the blades and thus coarse droplets are created (1 – 500 μm in diameter). Particularly coarse droplets are responsible for erosion of turbine blades because they are not accelerated to the vapour phase speed before impact with the rotor blade leading edge as depicted in the velocity diagram in Fig. 12. [16], [17], [18]

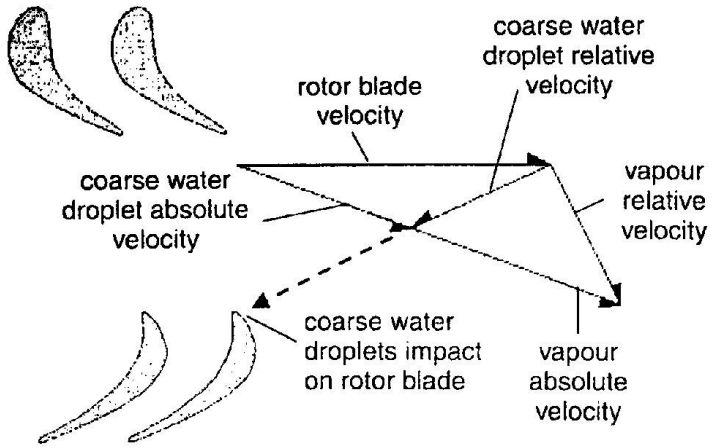

Figure 12: Velocity diagram of erosion process caused by coarse droplets [17]

4.1.1 Condensation

There are two basic condensation processes that can occur during the expansion, namely heterogeneous and homogeneous condensation. The combination of those two can occur too. The expansion speed, subcooling of the steam and the concentration of impurities in the steam affect which type of condensation takes place. [19]

4.1.1.1 Heterogeneous

Heterogeneous condensation occurs immediately after the crossing of the saturated vapour line or during a very low subcooling of the steam. The nuclei of water droplets start to condensate on the impurities which can be dust particles or a cluster of ions, for example. During the condensation, the heat is released and the subcooling decreases. This process acts against the expansion that increases the subcooling. If the expansion is slow or there are enough impurities in the steam, the process can be close to the thermodynamic equilibrium. [19]

4.1.1.2 Homogeneous

Homogeneous condensation takes place in cases when there are no impurities in the steam. The expansion causes that the steam is very subcooled. In this state, the steam is far from the equilibrium and therefore random clusters of molecules can cause the condensation as if they were impurities. [19]

The higher the subcooling the smaller impurities or clusters of molecules are needed. In the real steam, there are always some impurities and thus the heterogeneous condensation occurs first. If the number of impurities is small or the expansion process is too fast, the homogeneous condensation occurs as well. In some cases, the homogeneous condensation can be so sudden that it can be likened to the shock wave. This phenomenon appears particularly in flows through steam nozzles or channels between blades. During the sudden condensation, the number of droplets is constant and the only changing attribute is droplet diameter that is increasing. [19]

4.2 Wetness measurements

Wetness is the quantity of the liquid phase in wet steam relative to the to total quantity of both liquid and steam phases, which shows Eq. 24.

$$Y = \frac{m_l}{m_m} \ , \tag{24}$$

where Y is wetness, m_l is mass of liquid phase and m_m is mass of the whole mixture.

It can be easily measured by methods based on the thermodynamics principles. Methods utilizing light extinction has been under development in recent year, however such methods analyse fine droplets, which is, as previously mentioned, only part of the liquid

phase in wet steam. The other part is present in the form of coarse droplets and liquid films and must be measured separately. [16]

4.2.1 Thermodynamic methods

The principle is to transform a representative sample of the two-phase medium (wet steam) from the main flow into a single-phase medium (water or superheated steam) that can be measured outside the turbine. The wetness is then calculated from the balance of the heat transformation. There are three main techniques – throttling, heating and condensing. [16], [17]

Throttling transforms wet steam into superheated steam. The drying process follows an isenthalpic evolution from the high pressure at the sampling point to the low pressure in the auxiliary condenser. The superheat of 20°C at least is required in the auxiliary condenser to obtain sufficient heat transfer between two phases. [16]

Heating likewise throttling transforms wet steam into superheated steam. An electrical coil is used for drying wet steam. The complete evaporation process should be performed within the zone of electrical heating so that the losses due to throttling drying and external heat exchange are minimized and thus the heat balance is as accurate as possible. [16]

Condensing transforms the wet steam into liquid. Large heat exchangers are usually needed for this transformation and that is the reason why this technique is essentially applied on large mass flows. [16]

Although these methods are well-known, they have two main difficulties. Firstly, the acquisition of the representative sample that contains steam, fine droplets and coarse droplets is difficult. Secondly, the heat balance is not absolutely accurate due to heat losses in the connecting tubes or incomplete phase mixing, for example. Overall, the accuracy of thermodynamic methods is not very high but they are often the only way how to find out the value of wetness. [16]

4.2.2 Specific measurements in wet steam

The main task for such measurements is to determine the size and number distribution of droplets as well as their velocities. Methods using the electrical needles were used in the past, however they have been supplanted by optical methods that cover wide size range and provide higher reliability, accuracy and faster data acquisition and processing. The measurements should give data which could help to improve operational properties, reliability and efficiency of future turbines. [16], [20]

4.2.2.1 Fine droplets

The most common technique that is used for measuring the fine droplet (condensation fog) distributions utilizes extinction (attenuation) of the light beam. When the light passes

through the fog, a certain extinction can be observed. This phenomenon is described by Eq. 25 that is called the Lambert-Beer law and that defines the relationship between the attenuation of the light and the number and diameter of particles. [16], [19]

$$\frac{I}{I_0}=\exp\left(-\pi\cdot Q\cdot N\cdot L\cdot r_p^2\right) \quad , \tag{25}$$

where I_0 is the reference light intensity without any fog, I is the light intensity after passing the fog, L is the length of the section with the fog, N is the number concentration of droplets, r_p is the droplet diameter and Q is so called extinction factor. [19]

4.2.2.1.1 Two-wavelength method

Related to homogeneous condensation that takes place in the case of wet steam flow in nozzles, the number of droplets does not really change and thus the actual polydisperse system approximates to the monodisperse system. Therefore, the method utilizing the attenuation of the light of two different wavelengths can be used for the determination of the number of droplets and their diameters. Such a method is called the two-wavelength method. The ratio of two extinction factors is carried out after the measurements. From the Mie theory of light scattering, the function shape of the ratio in relation to the droplet radius is known and thus the droplet size can be determined. [19], [20]

4.2.2.1.2 One-wavelength method

The attenuation of one wavelength and the steam wetness is necessary to know for using one-wavelength method. The steam wetness can be determined by direct measurement or by calculation (e. g. using the expansion line in a h-s diagram). The wetness Y can be expressed as shown in Eq. 26.

$$Y=\frac{4}{3}\cdot\pi\cdot r_p^3\cdot\rho'\cdot\frac{N}{\rho} \quad , \tag{26}$$

where ρ' is the density of the liquid on the saturation line and ρ is the density of wet steam. The wet steam density follows Eq. 27.

$$\rho=\frac{\rho''}{1-Y} \quad , \tag{27}$$

where ρ'' is the density of the vapour on the saturation line.

Utilizing Eq. 25 – 27, the ratio $\frac{Q}{r_p}$ can be found and since the application of the Mie theory provides the function shape of the ratio in relation to the droplet radius again, the droplet size can be determined. [16], [18]

Both two-wavelength and one-wavelength methods are very accurate and their results can be consider as exact if the assumption of a monodisperse system is kept.

4.2.2.2 Coarse droplets

4.2.2.2.1 Shadowgraphy

Shadowgraphy is an optical method and has been proved to be very convenient for measuring coarse droplets. The goal of the measurement is to obtain a picture of the observed volume with droplets or their paths. [16]

The measuring probe consists of the camera, telecentric objective and front or back illumination. The magnification of the objective is limited by the minimal exposure time of the camera. The higher the magnification the better the resolution for small droplets, however the displacement of the droplet then can be out of the observed volume. Droplets appear as dark spots on the clear background but often they are blurred on the picture. The blurriness depends on the out-of-focus position of the droplet and its size. The length of the droplet's path on the picture and the exposure time make possible to compute the velocity of the droplet and determine the direction of the droplet's movement. [16], [20]

Taken pictures can be analysed by a computer and a size distribution can be determined as well as information about velocities of droplets. Calibration of the probe is needed for the correct pixel/dimension ratio. [16], [20]

4.2.2.2.2 Holography

Holography is optical method similarly to shadowgraphy, nevertheless there are some differences. Droplets are illuminated by a pulsed laser and the lens are not used at all. The interference between the light scattered by droplets and a reference beam is recorded on a sensitive plate which becomes the hologram of the droplets. After the record, the hologram image has to be reconstructed. The hologram is lit with a continuous laser beam and then the image of droplets can be observed and analysed. [16]

The main advantage is the capability to record droplets moving at high velocities of up to several hundreds metres per second. On the other hand, there is a requirement for the high quality and cleanliness of the optical system since there must be sufficient contrast between reference and object waves to obtain good hologram. Moreover, the whole procedure is rather time-demanding, which limits industrial application of this method. [16]

4.2.2.2.3 Other methods

Other methods used or tested for measuring coarse droplets utilize diffraction (described in the chapter 3.4) and scattering. Regarding scattering method, droplets scatter the initial laser beam at the focal area. The scattered beam is then collected by a lens and focused on the detector. The principle is to relate the light intensity measured by the detector to the droplet size. The higher the scattering the larger the droplet diameter. A white light source that provides homogeneous lighting is used for large droplets while a laser source with high light intensity is suitable for measuring small droplets. [16]

Methods utilizing both diffraction and scattering have some serious limitations. Regarding scattering methods, one of the most limiting factor is the coincidence effect when two or more droplets seem to be one large droplet. This happens particularly during measurements in steam turbines where the fog of fine droplets is found. That is the reason why the former mentioned methods are preferred, especially shadowgraphy. [16]

4.3 Other measurements

Among other quantities that are often measured in steam turbines belongs pressure and velocity of the medium.

Pressure in steam turbines is measured by using long probes that are inserted through fixed guide tubes. The probe can be up to 5 m long and the diameter is typically 25 mm. The steam flow between the probe head and the measuring device must be continuous, which brings the requirement of avoiding the water phase accumulation in the connecting lines. Accumulated water would distort the measuring. In order to keep the lines free from water, air is purging through. There are two ways, namely continuously and intermittent air purging. The former is rather complicated and therefore the latter is preferred. [16]

For velocity measurements in turbines, the Pitot tube principle is used. The dynamic pressure is measured and the velocity can be calculated following Eq. 28.

$$\Delta p = \frac{1}{2} \cdot \zeta \cdot \rho \cdot v^2 , \tag{28}$$

where Δp is dynamic pressure, which is the difference between the total pressure and the static pressure $(\Delta p = p_t - p_s)$, ζ is a coefficient depending on the probe shape, M is the flow Mach number, ρ is the flow density and v is the flow velocity. [16]

However, such a measurement have some difficulties. Firstly, the flow in the turbine is generally three-dimensional and thus the direction of the flow velocity is unknown. Secondly, both phases present in wet steam (vapour and droplets) interact with each other and these interactions must be taken into account as well. If there is only the condensation fog consisting of fine droplets, wet steam is considered to be a homogeneous medium since fine droplets are carried away with the speed of the flow. In the case that also coarse droplets are present, their mechanical effect in the vicinity of the probe head must be taken into account for the total pressure. Nevertheless, some corrections for data interpretation were developed and these measurements can be used as approximation at least. [16]

There were attempts to use photogrammetry for velocity flow measurements. However, it is not convenient to use photogrammetry in wet steam since fine droplets are too small to provide sufficient individual light scattering response that could be processed. And coarse droplets do not follow the steam flow and thus they cannot provide any information about flow velocity. [16]

5 Image evaluation

In low pressure parts of steam turbines, coarse droplets can move with the velocity higher than 200 m/s therefore the exposure time of the camera must be short enough so that a trace of the droplet might be captured. Taking into account the short exposure time, the frequency of the coarse droplet appearance is relatively low and thus thousands of pictures are taken in order to obtain one where the droplet trace is captured. It is not feasible to evaluated such a huge amount of images one by one manually, hence a computer program for the analyses have to be used. [18]

Images taken at the experimental facility designed in the other part of the thesis are meant to be evaluated by computers as well. A basic program for the evaluation was created in Matlab. Since the program was created before the experimental facility, it analyses images of other polydisperse samples. The images were captured in the Laboratory of turbines at the Department of Energy Engineering at Juliska by microscope Motic BA310.

5.1 Calibration

The developed program evaluates the images via pixels and therefore a calibration was necessary so that the final information is given in metric units. The goal of the calibration was to find out how many pixels constitute one millimetre. A calibration target in Fig. 13 made by Edmund Optics was used for the calibration. The picture of the target was made by the same microscope with the same setting as pictures of polydisperse systems in order to gain proper relationship between pixels and millimetres.

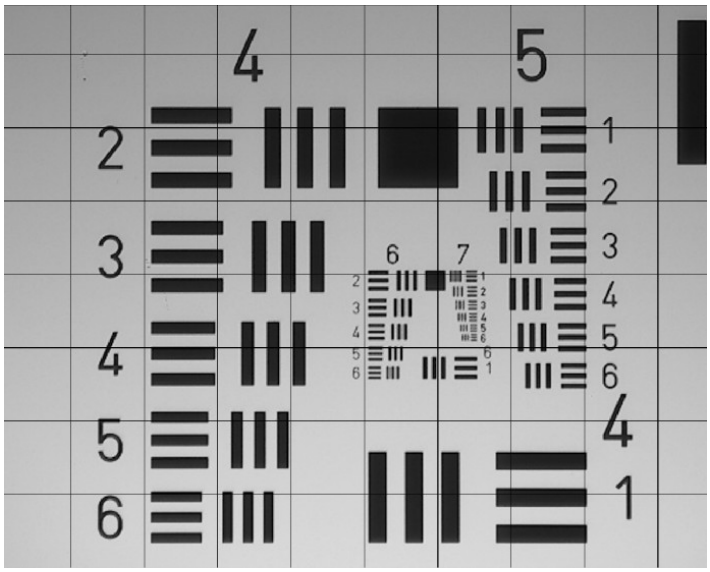

Figure 13: Calibration target

Each line pair (i.e. the black strip and gap) on the target has a precise dimension defined by the manufacturer. The number of pixels of the line pair was determined as shows the detail in Fig. 14.

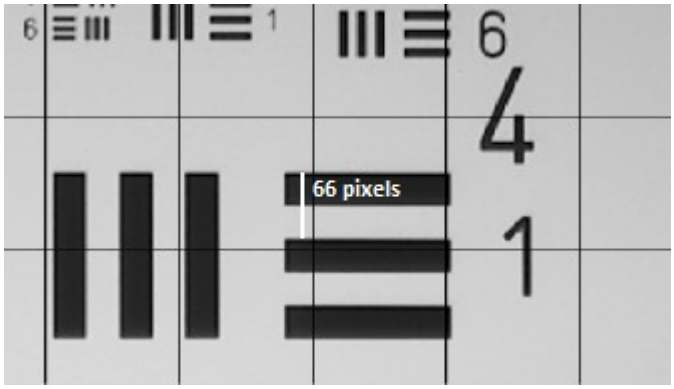

Figure 14: Detail of the calibration line pair

The dimension of this particular line pair is 1/16 mm according to manufacturer. Therefore, one pixel equals to 1/1056 mm and thus final results can be stated in metric units.

The number of pixels per line pair naturally depends on the magnification used during the image acquisition. The magnification of the stated example is ten. Nevertheless, the calibration process would be the same regardless the magnification.

Images captured by the microscope contain lines with a value of their length in μm that could be used for the calibration, too. However, their scales were not properly set before the picture was taken. Therefore, the calibration target was used instead.

5.2 Analysis of the glass powder

The first polydisperse system used for the analysis was glass powder consisting of spherical elements. The original image captured by the microscope is shown in Fig. 15.

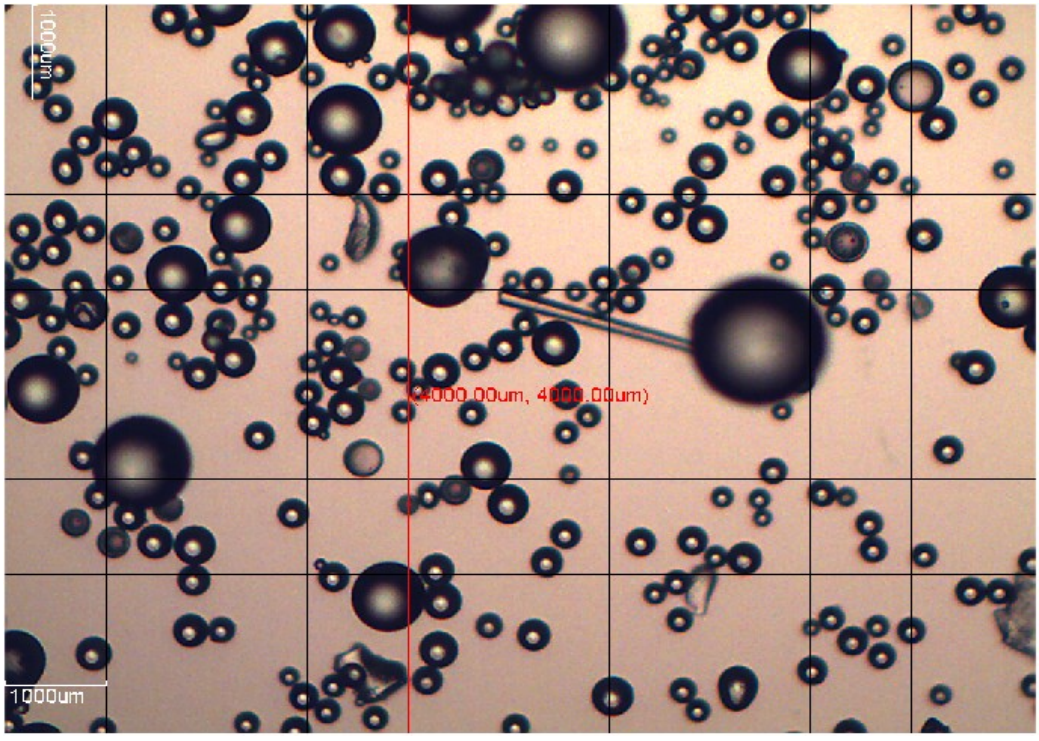

Figure 15: The original image of glass powder

As one can see, the microscope generates colour images, however, it is convenient to analyse high contrast images for a better object detection. Thus, the conversion to the greyscale and subsequently entirely black and white image was carried out as shown in Fig. 16 and 17.

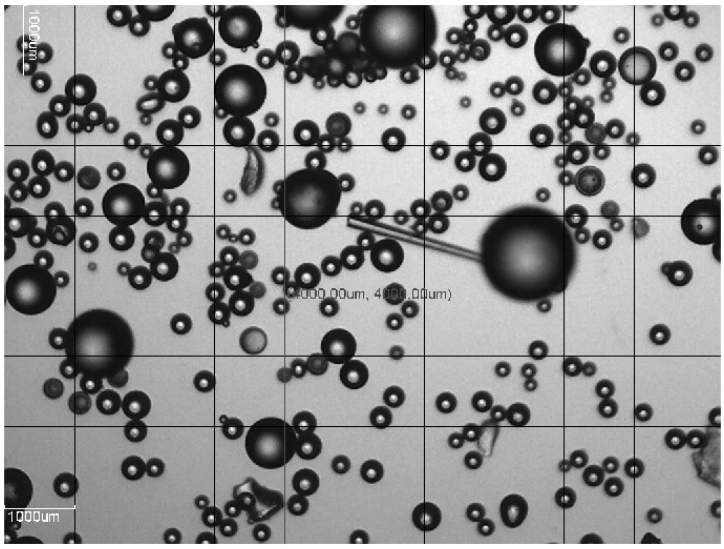

Figure 16: Greyscale image

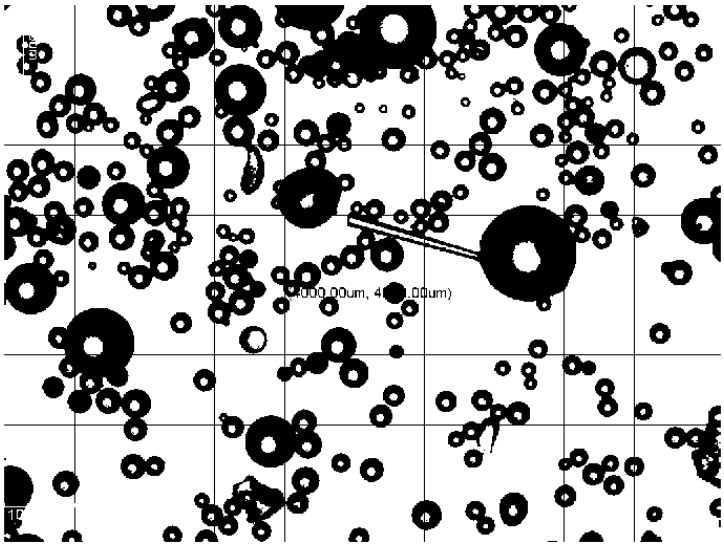

Figure 17: Black and white image

In following steps, the visible redundant grid was removed and the black and white colour were inverted because Matlab functions used in the algorithm consider that white pixels form objects and black pixels fill the background. Areas of the opposite colour inside objects were removed as well. The image after these steps, shown in Fig. 18, was analysed.

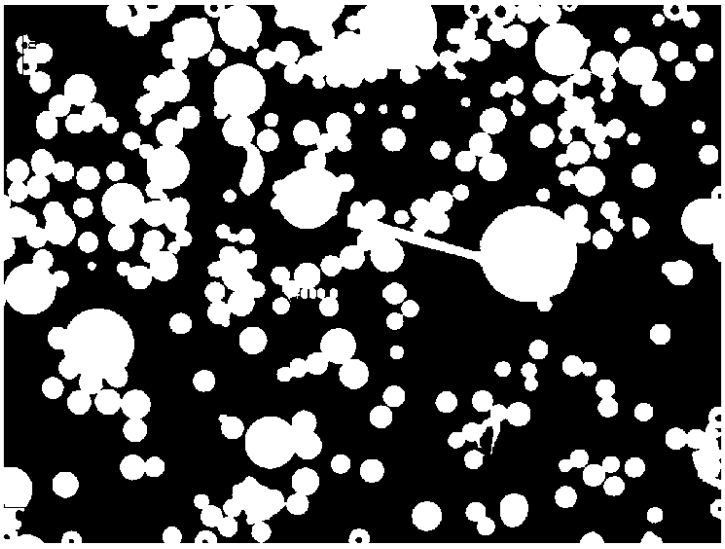

Figure 18: Image ready for the analysis

The analysis itself consisted of the boundary detection of white objects. Each continuous object was coloured and its area and perimeter were determined. In Fig. 19, the highlighted boundaries are obvious as well as the highlighting of the largest and smallest object with red and yellow colour, respectively.

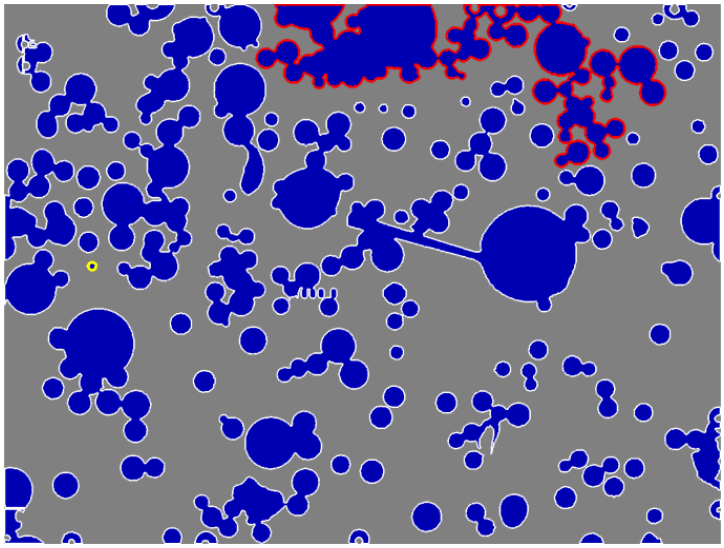

Figure 19: Analysed image

More important than the colour representation is processing of obtained data. In the algorithm, an index was assigned to each object and a graphical evaluation was performed using indices. In Fig. 20, there are three diagrams. The first diagram, marked as A, shows simply the value of area of each object in an order made automatically by Matlab. The second diagram B depicts the same values as diagram A but ordered from the lowest to the highest value. It provides basic information about the size distribution. The last diagram C is only a detailed depiction of the first part, specifically first ninety objects, of the diagram B. This detail shows more clearly the gradual increase in area values at the beginning of the diagram.

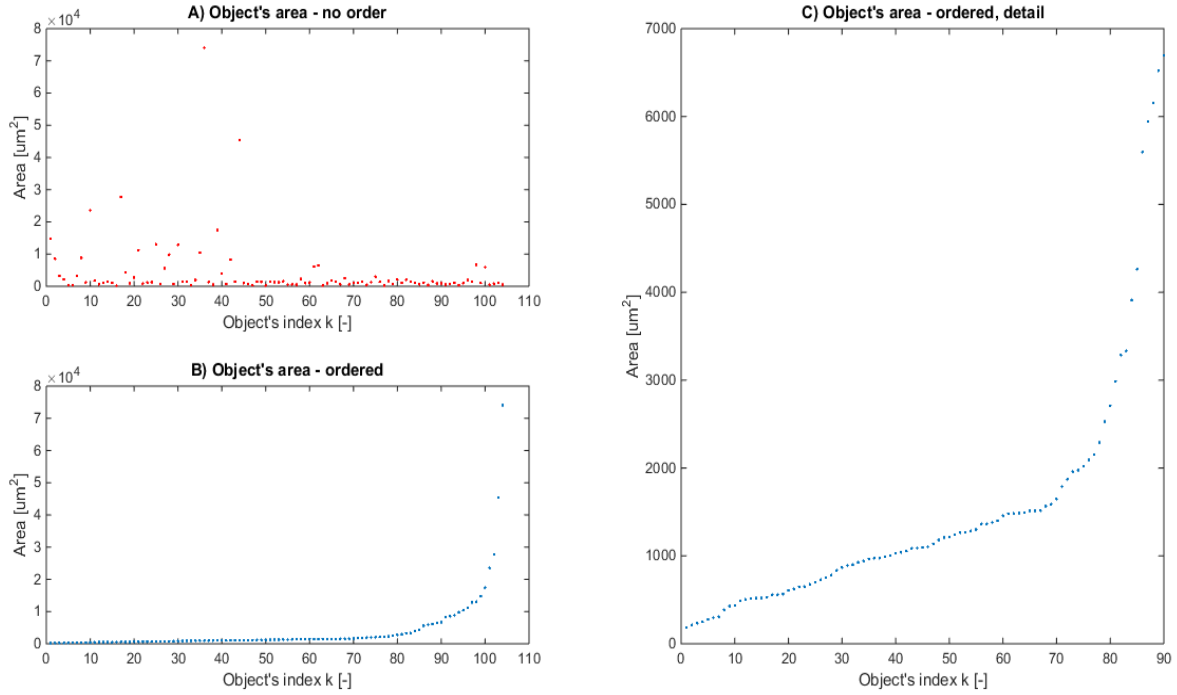

Figure 20: Diagrams of the analysed glass powder sample

Analogous diagrams could be made for perimeter values. They would have similar shapes, only values on the vertical axis would differ though.

Characteristics of each object were determined using prepared Matlab functions therefore the analysis of the polydisperse system described in paragraph 2.3 can be carried out as well. Diameters corresponding circles having the same area as objects in the image were determined. The analogous diameters were found out for the perimeter as well. Using these knowledge, the cumulative and complementary cumulative distribution function could be acquired from the sample. Since the exact number of objects and the respective characteristic values were known, the distribution functions were depicted using these pieces of information. In Fig. 21, there are the cumulative distribution function $F(d_a)$ and complementary cumulative distribution function $S(d_a)$. They were obtained as functions of the area based diameter d_a, which indicates the parameter in brackets. Similar functions might be found for the perimeter based diameter d_{pr} as well.

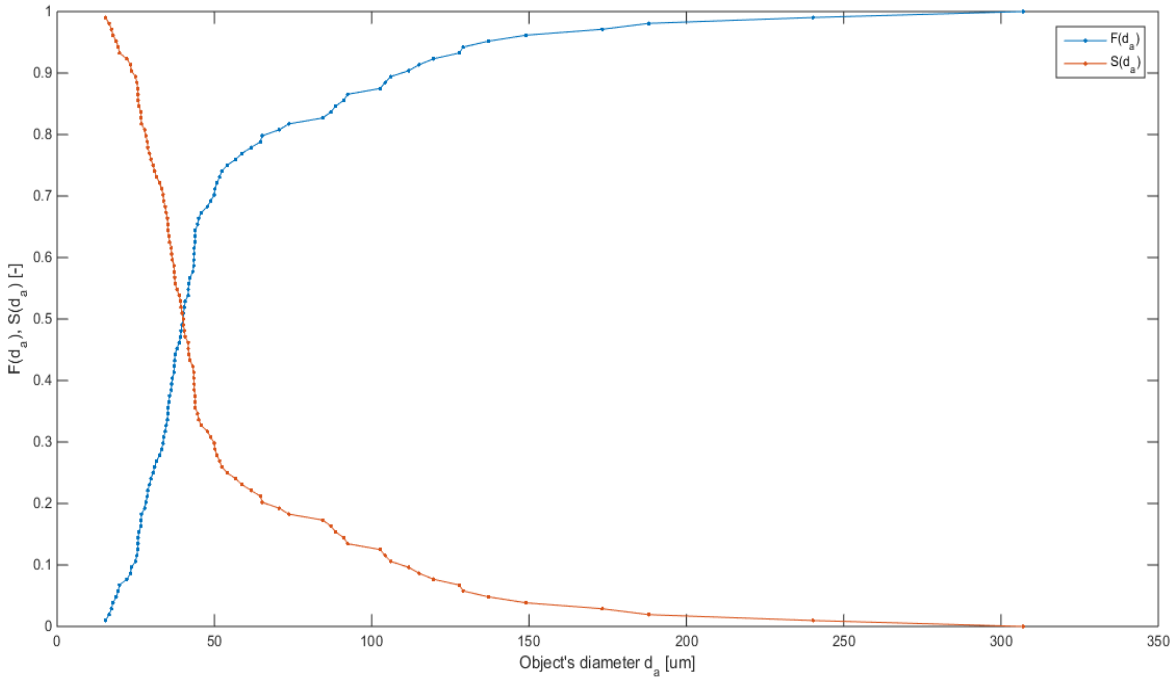

Figure 21: Cumulative and complementary cumulative distribution functions of the glass powder sample

The total number of objects on the image is known that is why diameters $d_{[1,0]}$, $d_{[2,0]}$, $d_{[3,0]}$ could be easily calculated. Calculation of Sauter $d_{[3,2]}$ and De Brouckere $d_{[4,3]}$ diameter was possible, too. All diameters were determined for both area and perimeter of objects and results rounded to the integer are stated in Tab. 3.

	Area diameters	**Perimeter diameters**
$d_{[1,0]}$ [µm]	55	46
$d_{[2,0]}$ [µm]	72	93
$d_{[3,0]}$ [µm]	93	159
$d_{[3,2]}$ [µm]	154	466
$d_{[4,3]}$ [µm]	210	616

Table 3: Diameters characterising the glass powder sample

The latter two diameters are very useful when the total number of particles in the sample is unknown. In this particular case, they are stated as informative. Diameters $d_{[1,0]}$, $d_{[2,0]}$, $d_{[3,0]}$ are also informative in this example, nevertheless, they might be important if some sub-sample with fewer objects were analysed and one characteristic value for the sub-system was needed.

A lot of other information can be acquired from the analysed set of objects, for example, statistical characteristics such as mean or median. Specific Matlab functions are available for this, which makes the acquisition relatively convenient. A few such characteristics are introduced in Tab. 4.

Statistical characteristics	
Number of objects [-]	104
Area of the smallest object [µm^2]	185
Area of the largest object [µm^2]	74060
Average area [µm^2]	4050
Area median value [µm^2]	1265

Table 4: Statistical values of the glass powder sample

In Fig. 22, there is another image of glass powder that was captured later and that was analysed, too. It was carried out especially in order to verify the capability of the program to evaluate polydisperse characteristics. Thus, the chosen sample contains a lot of objects that do not overlap each other very much.

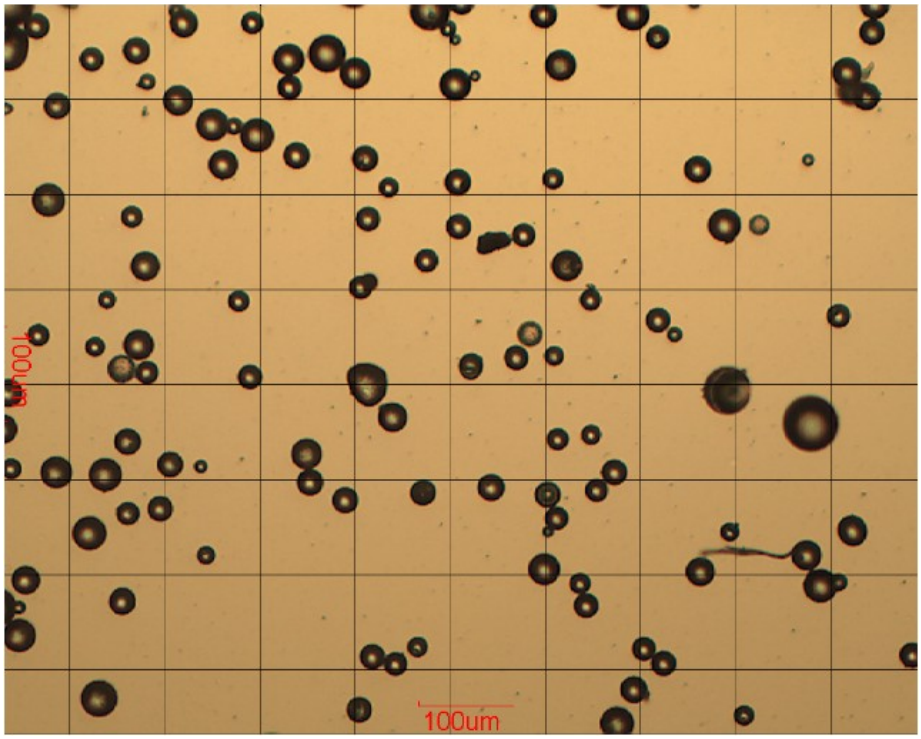

Figure 22: Image of the second glass powder sample

The same algorithm was used for the evaluation therefore the final image, which is shown in Fig. 23, looked in the same way.

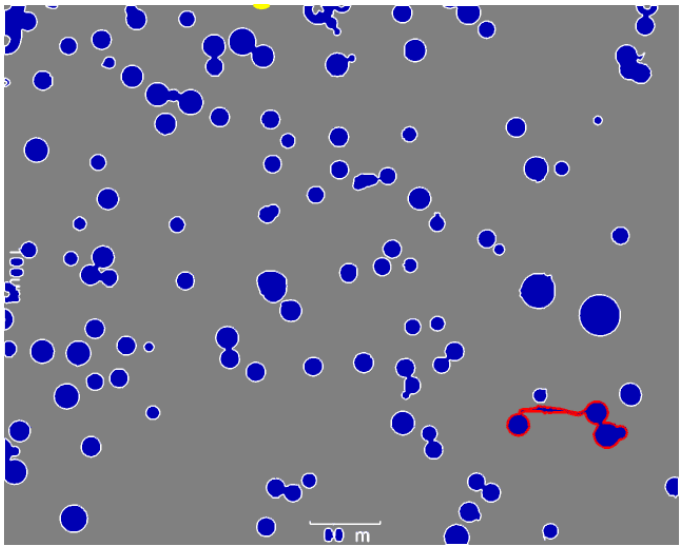

Figure 23: Analysed image of the second glass powder sample

The first graphical evaluation was performed using indices again. Three diagrams in Fig. 24 provide the same information as diagrams in the previous example. The diagram A shows the value of the area of each object in the order made automatically by Matlab. In the diagram B, there are the area values ordered from the lowest to the highest value. And the diagram C shows the detailed depiction of first ninety objects of the diagram B.

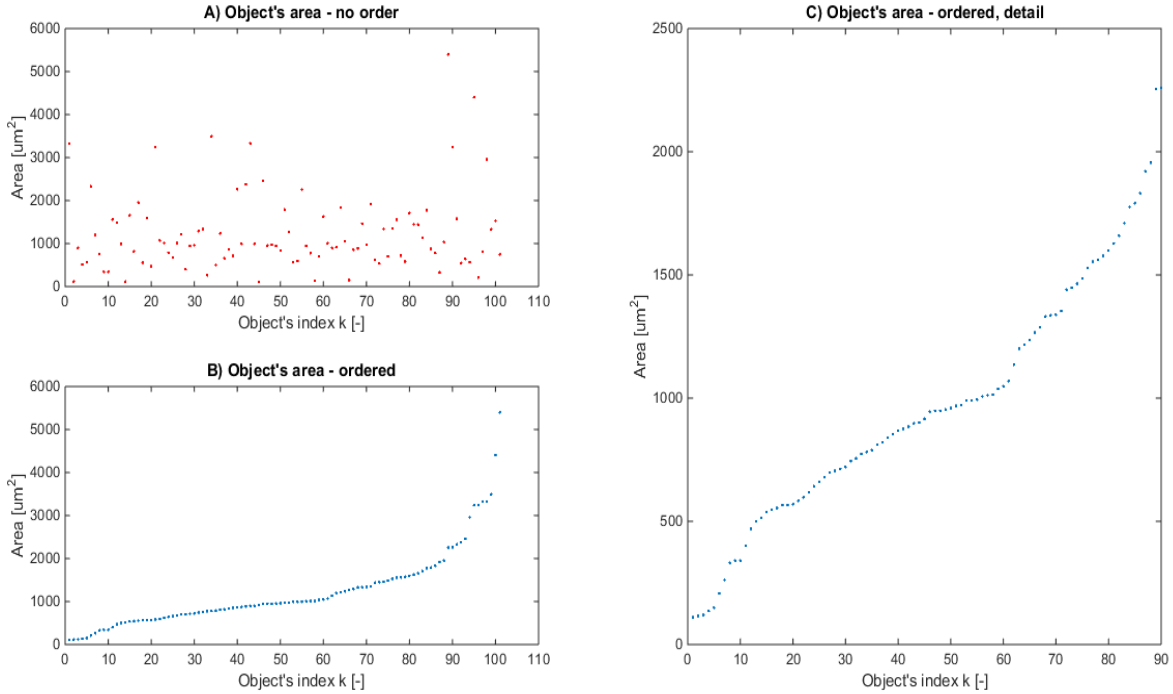

Figure 24: Diagrams of the second glass powder sample

The cumulative distribution function $F(d_a)$ and complementary cumulative distribution function $S(d_a)$ were depicted as well, which shows Fig. 25. They were obtained as functions of the area based diameter d_a again.

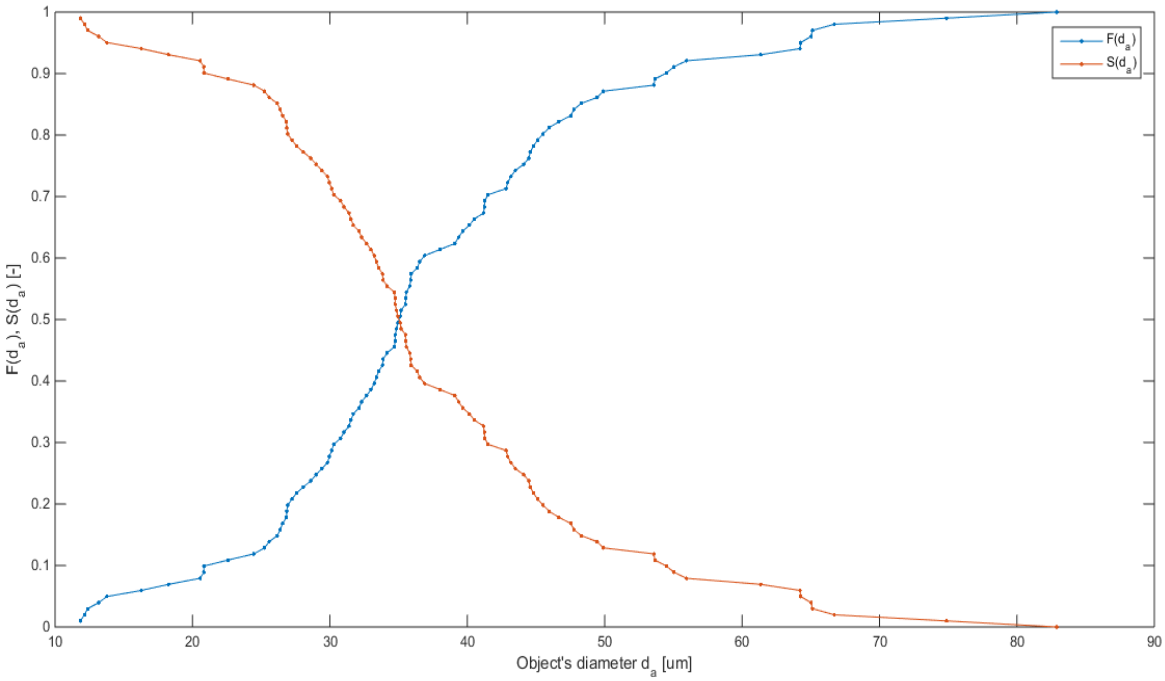

Figure 25: Cumulative and complementary cumulative distribution functions of the second glass powder sample

At first sight, these functions do not have so steep course in comparison to the first analysed image. It is caused mainly by the scale of the horizontal axis which is considerably larger regarding the second sample. The first image had a few very large objects with a diameter bigger than 100 μm while the biggest object on the second image had the diameter smaller than 90 μm. That is the reason for a different look of the distribution functions.

Identically to the first image analysis, diameters $d_{[1,0]}$, $d_{[2,0]}$, $d_{[3,0]}$ were calculated as well as Sauter $d_{[3,2]}$ and De Brouckere $d_{[4,3]}$ diameters. All diameters were determined for both area and perimeter of objects again and results rounded to the integer are stated in Tab. 5.

	Area diameters	**Perimeter diameters**
$d_{[1,0]}$ [μm]	37	22
$d_{[2,0]}$ [μm]	40	25
$d_{[3,0]}$ [μm]	42	30
$d_{[3,2]}$ [μm]	47	43
$d_{[4,3]}$ [μm]	52	64

Table 5: Diameters characterising the second glass powder sample

Diameter values were smaller compared to the first image, especially Sauter and De Brouckere diameters. The reason were smaller objects on the second image of course. The low values of the latter two diameters are caused by the absence of very large objects (more than 100 μm) that significantly affect the final value due to the calculation with their third or fourth power.

At last, a few statistical characteristics were obtained and they are introduced in Tab 6.

Statistical characteristics	
Number of objects [-]	101
Area of the smallest object [μm^2]	110
Area of the largest object [μm^2]	5389
Average area [μm^2]	1228
Area median value [μm^2]	968

Table 6: Statistical characteristics of the second glass powder sample

5.3 Analysis of ground coal

The algorithm was tested on another samples too. However, the other sample did not contain circular objects but randomly shaped elements. A sample of ground coal was used for obtaining the image that is in Fig. 26. This image has higher magnification than previous images, specifically 40. After the calibration, it was defined that one pixel corresponds to 1/3264 mm.

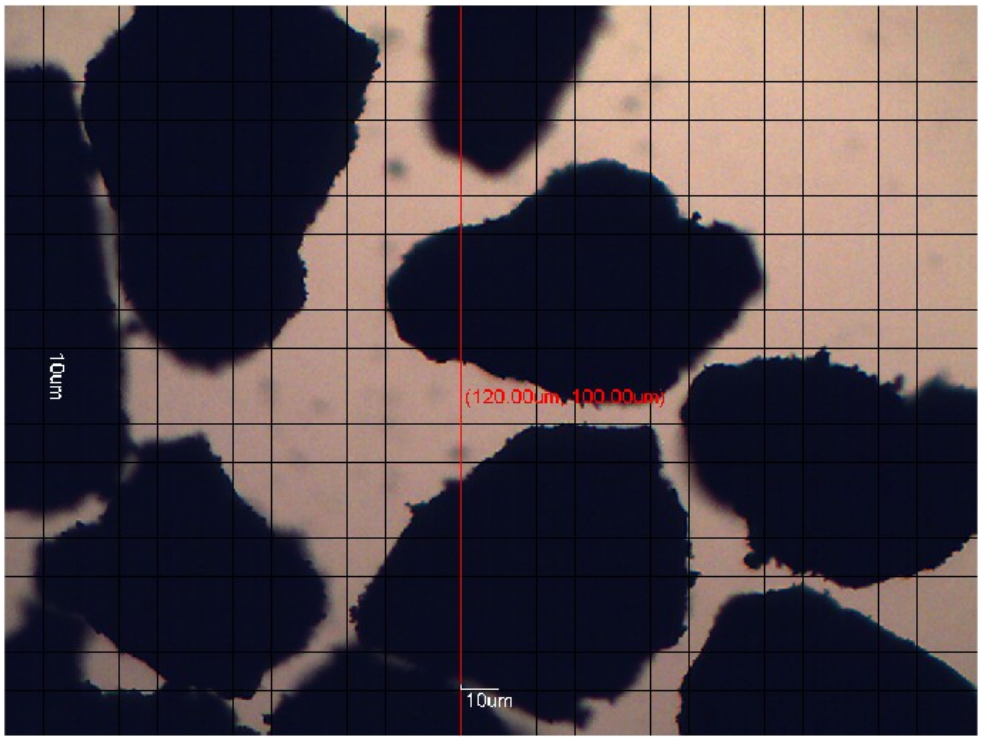

Figure 26: The original image of ground coal

The processing procedure was identical therefore the analysed picture in Fig. 27 looked in the same way. The largest object was highlighted by the red and the smallest by the yellow colour again.

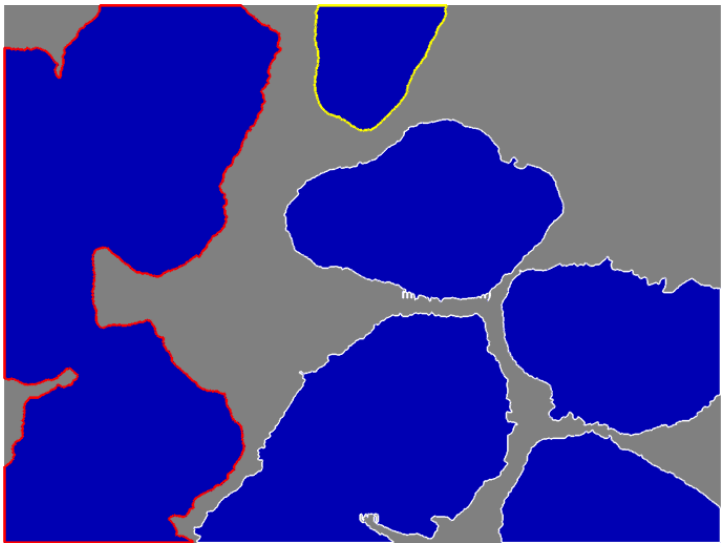

Figure 27: Analysed image of ground coal

In Fig. 28, there are diagrams that provide the same information as diagrams at previous images. The diagram A shows the area value of each object in the automatic order. The diagram B depicts these values ordered from the lowest to the highest value. However, in this case it does not provide information about the size distribution since there are only six objects on the picture and it cannot be taken as a representative sample. Moreover, there is only one object of a full shape, others are reduced by image edges.

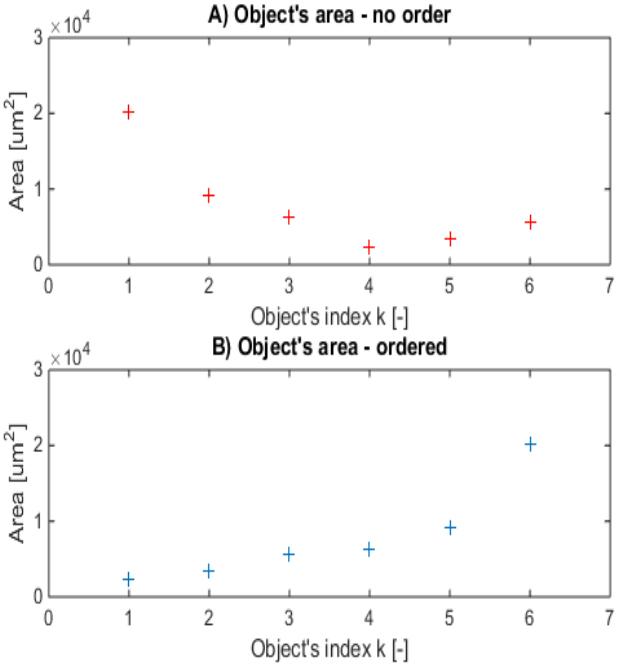

Figure 28: Diagrams of the ground coal sample

The program depicted the distribution functions $F(d_a)$ and $S(d_a)$ as well, as one can see in Fig. 29. Nevertheless, they are not conclusive for the same reason as mentioned above, which is the small number of objects.

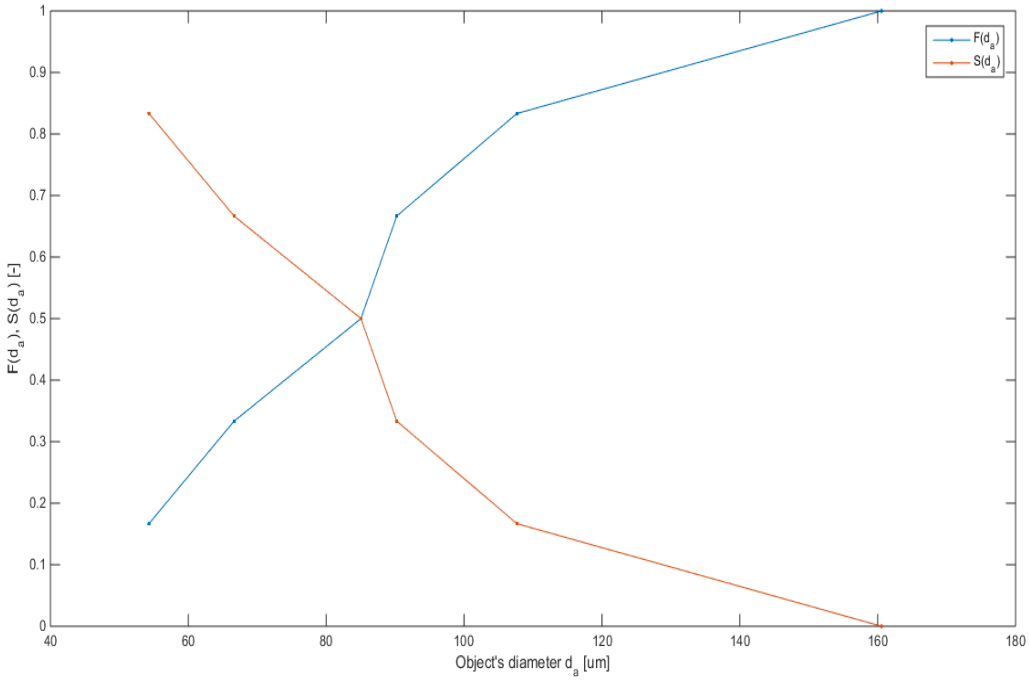

Figure 29: Distribution functions of the ground coal sample

All diameters stated in the previous image analysis were determined again. Their values are in Tab. 7.

	Area diameters	**Perimeter diameters**
$d_{[1,0]}$ [µm]	94	69
$d_{[2,0]}$ [µm]	100	79
$d_{[3,0]}$ [µm]	106	88
$d_{[3,2]}$ [µm]	120	110
$d_{[4,3]}$ [µm]	132	126

Table 7: Diameters characterising the ground coal sample

Statistical characteristics of the ground coal sample are introduced in the Tab. 8.

Statistical characteristics	
Number of objects [-]	6
Area of the smallest object [µm^2]	2315
Area of the largest object [µm^2]	20248
Average area [µm^2]	7872
Area median value [µm^2]	6038

Table 8: Statistical values of the ground coal sample

Since the sample of the ground coal was not suitable for obtaining polydisperse characteristics, a new image of another ground coal sample was captured. The image is shown in Fig. 30. The sample contained more objects that did not overlap each other very much.

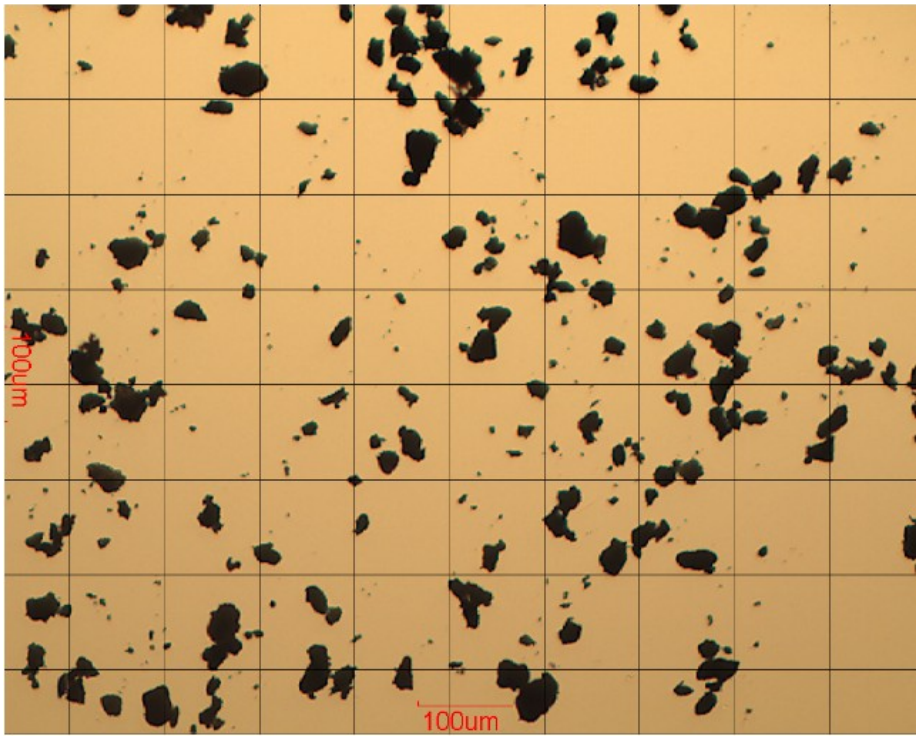

Figure 30: Image of the second ground coal sample

The evaluating process was identical to all previous examples. The final analysed image is shown in Fig. 31.

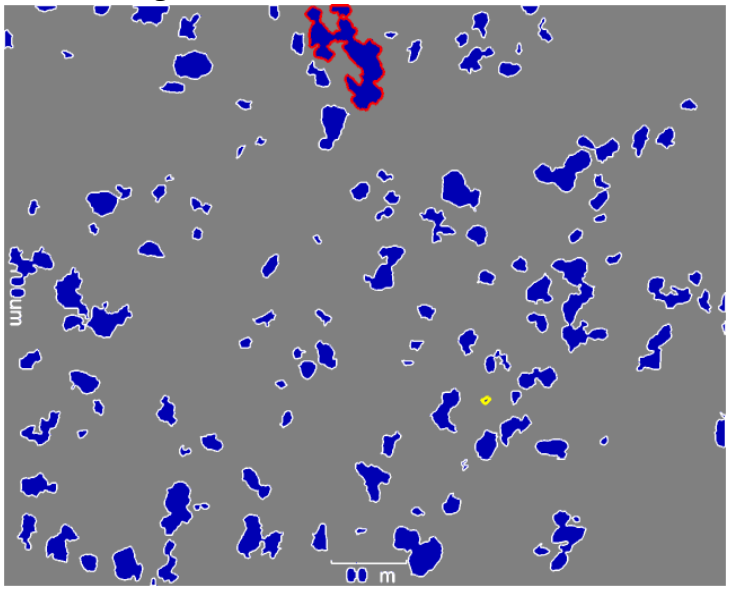

Figure 31: Analysed image of the second ground coal sample

In Fig. 32, there are diagrams giving the same information as at previously analysed images. The diagram A shows the area value of each object in the automatic order by

Matlab in relation to indices. The diagram B depicts these values ordered from the lowest to the highest value. The diagram C shows the detail of first ninety points of diagram B.

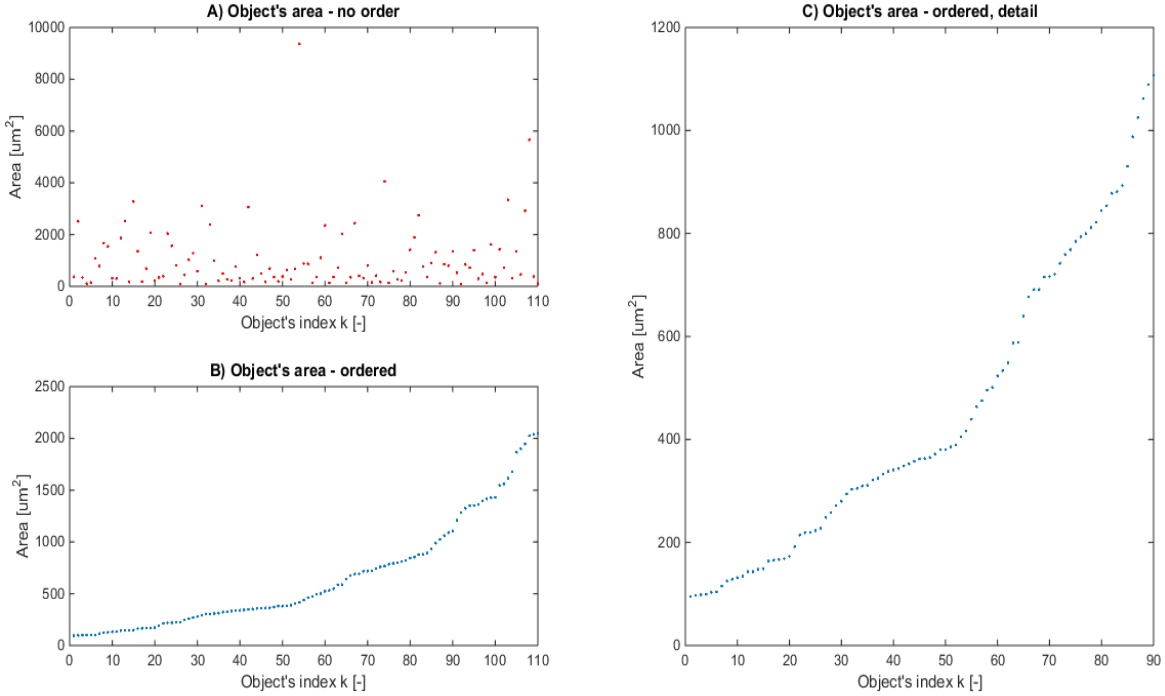

Figure 32: Diagrams of the second ground coal sample

Subsequently, cumulative and complementary cumulative distribution functions were made, which shows Fig 33.

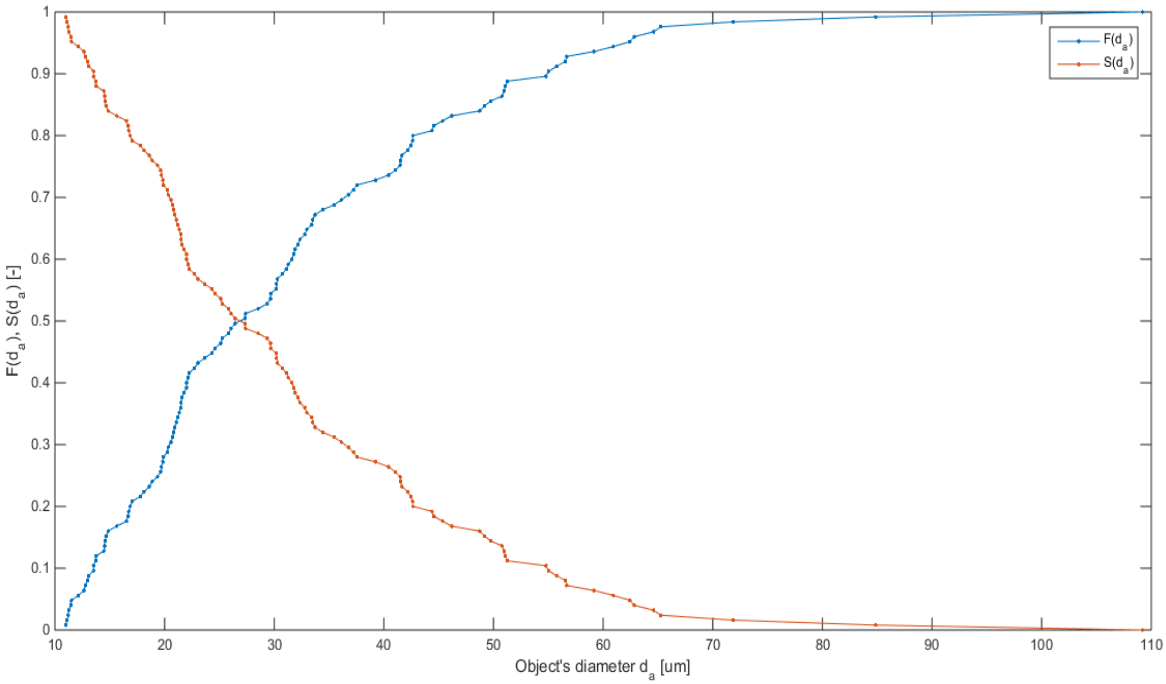

Figure 33: Distribution functions of the second ground coal sample

Naturally, all the imaginary diameters were obtained as well. They are stated in Tab. 9.

	Area diameters	Perimeter diameters
$d_{[1,0]}$ [μm]	31	22
$d_{[2,0]}$ [μm]	36	29
$d_{[3,0]}$ [μm]	40	38
$d_{[3,2]}$ [μm]	51	66
$d_{[4,3]}$ [μm]	62	99

Table 9: Diameters of the second ground coal sample

Finally, the statistical characteristics of the sample, that are introduced in Tab. 10, were acquired too.

Statistical characteristics	
Number of objects [-]	125
Area of the smallest object [μm^2]	95
Area of the largest object [μm^2]	9364
Average area [μm^2]	991
Area median value [μm^2]	687

Table 10: Statistical characteristics of the second ground coal sample

5.4 Suggestions for improvements

There are several options for a better precision of the final results. In Fig. 15, there is evident that some objects are not perfectly sharp. This blurriness is caused by the object position in relation to the focus point of the microscope lens. The focus point was adjusted for middle sized objects and thus both very small and very large objects are blurry since they lie behind or in front of the focus point, respectively. The blurriness could be eliminated by adding a suitable algorithm in the program. Another increase of the analysis precision could be reached in during conversion process from the greyscale to the entirely black and white image. A value defining the threshold between the black and white colour is set during the process. This threshold value might be optimized so that object borders are changed as little as possible compared to the original state.

Particles of some testing samples are overlapping each other therefore areas of obtained objects does not correspond to a single particle. Naturally, the area distribution in this case is not the correct area distribution of the polydisperse system. This drawback might be removed by implementing appropriate algorithm, however, it is not necessary for the coarse droplets analysis. As mentioned previously, the concentration of coarse droplets is rather low and it is expected to capture a single coarse droplet on one of thousands taken pictures, hence there will be no overlapping objects.

5.5 Conclusion

This Matlab program was made as a suggestion how acquired images could be analysed.

Analysed images of the glass powder sample provide good results regarding the object detection as well as subsequent gaining of distribution characteristics. The first image of the ground coal sample confirmed the capability of the program to detect objects, which was crucial. Since distribution characteristics were inconclusive, which was caused by the small number of objects on the image, another image of the ground coal sample was acquired. The analysis of the last sample confirmed the functionality of the program regarding distribution characteristics.

Though the program was successfully tested on four different images, there are still needed some improvements in the program that will enhance the precision of the analysis. Nevertheless, these improving steps implemented in the algorithm would be convenient to test on images similar to the coarse droplets pictures. However, the program does not have to be used strictly for analysing coarse droplets. It contains a basic algorithm that could be adjusted for analysing coarse droplets as well as other polydisperse systems. Adjustments and improvements are needed either way. Eventually, a user-friendly interface could be created for the Matlab code.

6 Design of the experimental wind tunnel

As mentioned previously, the program for the image evaluation was developed primarily for the analysis of course droplets. However, the images containing coarse droplets cannot be acquired easily by a microscope and therefore a wind tunnel for simulating the coarse droplets formation was designed. The photogrammetric probe that has been developed within the research at the Department of Energy Engineering will capture the images.

6.1 Wind tunnel background search

A wind tunnel is a device utilized for an investigation of aerodynamic properties of a certain object. They has been widely used in aviation or automotive, but nowadays they represent a crucial instrument in other research areas where aerodynamics is important, too. In a simplified way, a wind tunnel is a tunnel through which air or some other gas flows. Effects of the investigated object on the stream are being determined. [21]

There are a wide variety of wind tunnels. Each wind tunnel is designed for a specific purpose and speed range. Some wind tunnels are very large therefore objects in life-size can be placed inside. The flow speed in such tunnels is not very high and reaching the supersonic speed is essentially impossible. In order to examine processes at high or even supersonic speed, small wind tunnels are built. Small tunnels do not allow to investigate properties of life-size objects and therefore only their small models are used. Similitude parameters are then used for the conversion of model properties to properties of the life-size object. [21]

Wind tunnels consist of several sections that usually are a confuser, diffuser and measuring section itself that is situated in the place with the highest flow speed. The investigated object is located in the measuring section. Designs of the subsonic and supersonic tunnel are different as shows Fig. 34. [22]

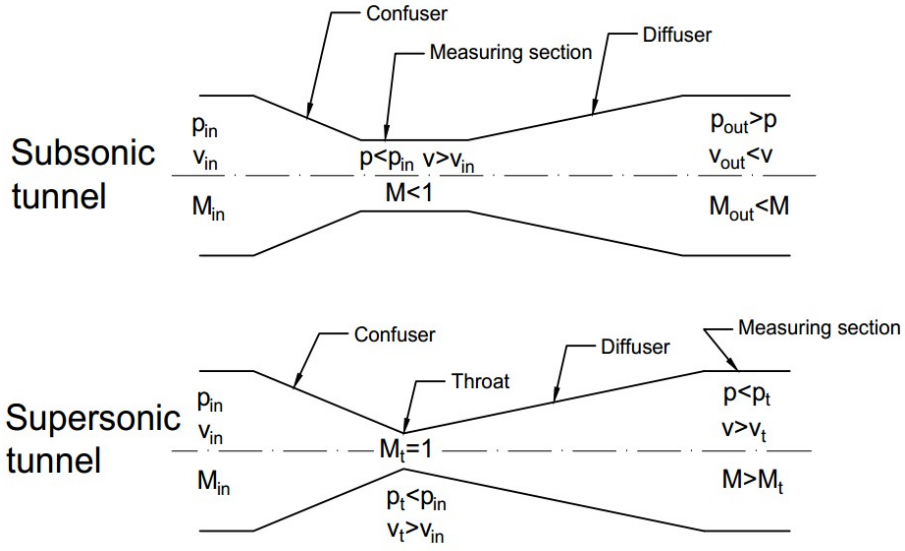

Figure 34: Designs of subsonic and supersonic tunnels

The subsonic tunnel has the measuring section right behind the contracting confuser. Decreasing the cross-section increases the velocity and decreases the pressure of the flow. Relating to the subsonic velocities, increasing of the cross-section causes a decrease of the flow velocity and increase of the pressure. Therefore, the measuring section is placed right behind the contracting part. On the other hand, increasing of the cross-section increases the velocity of the flow and decreases the pressure in the case of supersonic tunnels if the flow was choked (Mach number = 1 and the flow cannot be accelerated by a decrease of the cross-section any more) before. That is why, the measuring section in supersonic tunnels is placed behind the diffuser. There are other accessories in wind tunnels, such as flow straighteners before the measuring section or heat exchangers in some cases. [22], [23]

There are two main types of wind tunnels and that are open and close tunnels. In open wind tunnels, the flowing gas goes through the measuring section and leaves the tunnel, while, in close wind tunnels, the gas after the passing the measuring section is led back in front of the measuring section in a close loop. The flow through the tunnel is usually provided by a fan but sometimes a pressure vessel is used instead. [23]

6.2 Objectives for a design of the wind tunnel

The flowing medium through the experimental wind tunnel can be either hot steam or air. The flow speed should be very high, ideally supersonic, since such high speeds occur in steam turbines. The tearing away process of coarse water droplets should be simulated in the tunnel. Therefore, an object is situated in the tunnel channel in the transverse direction to the flow. A water film forms on that object and subsequently droplets tear away. Airfoil NACA 0008 was chosen as the object. In the case of the flowing air, there is a groove in the airfoil for a water supply so that the film can form. In this arrangement, water can be easily replaced by some other liquid.

The experimental facility is placed in the Laboratory of turbines of Energy Engineering Department at Juliska. There is a hot steam supply in the laboratory that could be used. The pressure of the hot steam is 0,6 MPa. Regarding the air flow, it is provided by the air tank that is in the laboratory. The air tank's volume is 0,5 m^3 and the maximal permissible pressure in the tank is 0,6 MPa.

This thesis deals with air as flowing medium. Hot steam, that will provide better approximation of a real state in last stages of low pressure steam turbines, will be utilized in a next step of the research.

6.3 Description of the test facility

The test facility is shown in Fig. 35 and it consists of the air tank, settling chamber, measuring chamber and camcorders for capturing pictures. The purpose of the settling chamber is to calm down the air flow from the tank in order to obtain the flow through the

measuring chamber with as few disturbances as possible. The settling chamber is connected to the measuring chamber containing a nozzle shaped channel in which the airfoil is situated. A small amount of water is supplied on the airfoil in order to create a thin water film. The nozzle is made in order to accelerate the air flow, which causes tearing away of water droplets from the airfoil. The tearing away process is captured by camcorders and acquired pictures can be subsequently analysed. Last but not least, the test facility is equipped with measuring instruments. In the settling chamber, there are instruments for measuring the temperature and static pressure. The static pressure is measured in the measuring chamber close to the airfoil as well.

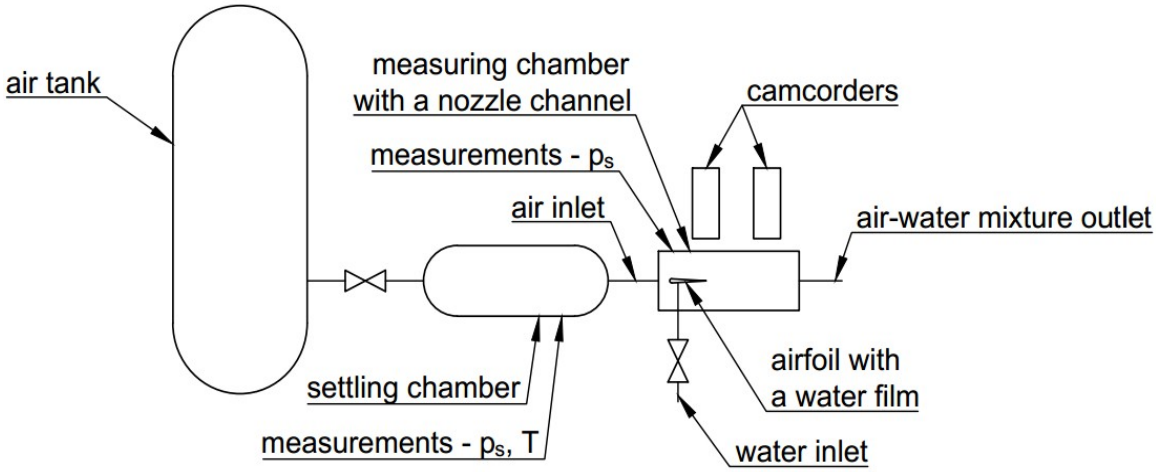

Figure 35: Test section scheme

A similar experiment was carried out in [24] where the air flow velocity was about 30 m/s during the experiment. However, the velocity of the working fluid in a steam turbine can reach hundreds m/s (can be even supersonic) and therefore the measuring chamber was intended to be designed for higher air flow velocity.

6.4 Basic calculation of the nozzle for air

The calculation was carried out in order to find out whether the supersonic speed of the flow can be reached for a reasonable period of time. Inputs for the calculation were the pressure in the air tank, its volume and the air temperature in the tank that was assumed to be 25°C. Air is considered to be the ideal gas in the calculation.

At first, the density and total air mass in the tank were calculated following Eq. 29 and 30.

$$\rho_0 = \frac{p_0}{r \cdot T_0} = \frac{6 \cdot 10^5}{287{,}1 \cdot 298{,}15} = 7{,}009\ kg/m^3 \qquad (29)$$

$$m_0 = \rho_0 \cdot V_0 = 7{,}009 \cdot 0{,}5 = 3{,}505\ kg \qquad (30)$$

The tube that leads air from the air tank to the settling chamber has the diameter of 8 mm. This diameter was considered to be the critical diameter and time of the duration of the

critical flow through the cross section was calculated. The critical flow is the state of the flow when its speed reaches the sonic speed.

The critical flow speed can be calculated from Eq. 31.

$$c^* = \sqrt{\kappa \cdot r \cdot T^*} \ , \tag{31}$$

where critical temperature T^* can be derived from the law of conservation of energy. For the adiabatic flow without gaining the technical work, the law in its integral form is shown in Eq. 32.

$$h^* + \frac{(c^*)^2}{2} = h_0 + \frac{(c_0)^2}{2} \ , \tag{32}$$

where flow speed c_0 in the air tank is considered to be zero, enthalpies h^* and h_0 can be expressed according to Eq. 33.

$$h = c_p \cdot T \tag{33}$$

The law of conservation of energy after mentioned operations is in Eq. 34.

$$c_p \cdot T^* + \frac{(c^*)^2}{2} = c_p \cdot T_0 \tag{34}$$

Using Eq. 35 and 36, c_p can be expressed by Eq. 37.

$$\frac{c_p}{c_v} = \kappa \tag{35}$$

$$c_p - c_v = r \tag{36}$$

$$c_p = \frac{\kappa \cdot r}{\kappa - 1} \tag{37}$$

Inserting Eq. 31 and 37 in Eq. 34, the law can be written as Eq. 38.

$$\frac{\kappa \cdot r}{\kappa - 1} \cdot T^* + \frac{\kappa \cdot r \cdot T^*}{2} = \frac{\kappa \cdot r}{\kappa - 1} \cdot T_0 \tag{38}$$

After the adjustment, critical temperature T^* can be expressed in the form of Eq. 39.

$$T^* = \frac{2}{\kappa + 1} \cdot T_0 \tag{39}$$

Using Eq. 31 and Eq. 39, the critical flow speed can be calculated as shows Eq. 40.

$$c^* = \sqrt{\frac{2 \cdot \kappa}{\kappa + 1} \cdot r \cdot T_0} = \sqrt{\frac{2 \cdot 1{,}4}{1{,}4 + 1} \cdot 287{,}1 \cdot 298{,}15} = 316{,}015 \, m/s \tag{40}$$

The critical pressure ratio defines the ratio of pressures after and before the nozzle at which the sonic speed in the narrowest part of the nozzle is reached. In the case of a convergent nozzle, decreasing of this ratio below the critical value does not lead to an increase of the flow speed any more. The critical pressure ratio for air can be derived from Eq. 39 that can be written in the form of Eq. 41 if the ideal gas law in Eq. 29 is used.

$$p^* \cdot v^* = \frac{2}{\kappa+1} \cdot p_0 \cdot v_0 \quad (41)$$

With the knowledge of Eq. 42, that is valid for adiabatic processes, specific volumes v^* and v_0 can be eliminated and the critical pressure ratio can be calculated following Eq. 43.

$$p^* \cdot (v^*)^\kappa = p_0 \cdot (v_0)^\kappa \quad (42)$$

$$\frac{p^*}{p_0} = \left(\frac{2}{\kappa+1}\right)^{\frac{\kappa}{\kappa-1}} = \left(\frac{2}{1{,}4+1}\right)^{\frac{1{,}4}{1{,}4-1}} = 0{,}528 \quad (43)$$

The critical pressure after the nozzle was calculated using the critical pressure ratio as shows Eq. 44.

$$p^*_{out} = \left(\frac{2}{\kappa+1}\right)^{\frac{\kappa}{\kappa-1}} \cdot p_0 = 0{,}528 \cdot 600 = 316{,}8\, kPa \quad (44)$$

The critical specific volume and critical mass flow were determined using Eq. 45 (derived from Eq. 42) and the continuity equation written in Eq. 46, respectively.

$$v^* = \frac{1}{\rho} \cdot \left(\frac{p_0}{p^*_{out}}\right)^{1/\kappa} = \frac{1}{7{,}009} \cdot \left(\frac{600}{316{,}8}\right)^{1/1{,}4} = 0{,}225\, m^3/kg \quad (45)$$

$$\dot{m}^* = S^* \cdot c^* \cdot \frac{1}{v^*} = \frac{\pi \cdot 0{,}008^2}{4} \cdot 316{,}015 \cdot \frac{1}{0{,}225} = 0{,}0706\, kg/s \quad (46)$$

This critical mass flow is obviously dependent on conditions of air in the tank that change over time. Therefore, new values of the air mass m_0 , pressure p_0 and density ρ_0 in the tank, critical pressure after the nozzle p^*_{out} , critical specific volume v^* and critical mass flow $\dot{m}^*$ were calculated every two seconds and were put in Tab. 11.

t [s]	m_0 [kg]	ρ_0 [kg/m3]	v^* [m^3/kg]	$\dot{m}^*$ [kg/s]	p_0 [kPa]	p^*_{out} [kPa]
0	3,505	7,009	0,225	0,0706	600	316,800
2	3,364	6,727	0,235	0,0677	575,842	304,044
4	3,228	6,456	0,244	0,0650	552,656	291,802
6	3,098	6,196	0,255	0,0624	530,404	280,053
8	2,973	5,947	0,265	0,0599	509,047	268,777
10	2,854	5,707	0,276	0,0575	488,551	257,955
12	2,739	5,478	0,288	0,0551	468,880	247,569
14	2,629	5,257	0,300	0,0529	450,001	237,600
16	2,523	5,045	0,313	0,0508	431,882	228,034
18	2,421	4,842	0,326	0,0487	414,493	218,852
20	2,324	4,647	0,340	0,0468	397,803	210,040
22	2,230	4,460	0,354	0,0449	381,786	201,583
24	2,140	4,281	0,369	0,0431	366,414	193,466
26	2,054	4,108	0,384	0,0414	351,660	185,677
28	1,971	3,943	0,400	0,0397	337,501	178,201
30	1,892	3,784	0,417	0,0381	323,912	171,026
32	1,816	3,632	0,435	0,0366	310,870	164,139
34	1,743	3,485	0,453	0,0351	298,353	157,530
36	1,673	3,345	0,472	0,0337	286,340	151,188
38	1,605	3,210	0,492	0,0323	274,811	145,100
40	1,541	3,081	0,512	0,0310	263,746	139,258
42	1,479	2,957	0,534	0,0298	253,126	133,651
44	1,419	2,838	0,556	0,0286	242,934	128,269
46	1,362	2,724	0,579	0,0274	233,153	123,105
48	1,307	2,614	0,604	0,0263	223,765	118,148
50	1,254	2,509	0,629	0,0253	214,755	113,391
52	1,204	2,408	0,655	0,0242	206,108	108,825
54	1,155	2,311	0,683	0,0233	197,810	**104,444**
56	1,109	2,218	0,712	0,0223	189,845	**100,238**
58	1,064	2,129	0,741	0,0214	182,201	96,202
60	1,021	2,043	0,772	0,0206	174,865	92,329

Table 11: Change of air and flow quantities over time

From Tab. 11, one can see that the condition for the critical flow, which is the critical pressure after the nozzle higher than the atmospheric pressure, would not be fulfilled approximately after 55 seconds.

The requirement of 60 seconds was not met, nevertheless the difference is not very high and it could be accepted. But, the diameter of 8 mm is too tiny for the measuring section, and moreover, no pressure losses, that would decrease the calculated time, were considered in the calculation. For these reasons, the supersonic air flow will not be reached during the first experiment. In future experiments, the supersonic speed of the air flow could be possible if the inlet tube has a bigger diameter than current 8 mm and a compressor is in operation during the experiment. In the case of hot steam, there is no limitation due to the storage tank or small tubes and therefore the supersonic speed could be reached.

Rectangle cross section of the width of 15 mm and height of 20 mm was set as the smallest cross section of the nozzle.

6.5 Design elements

Since the test facility is situated in the Laboratory of turbines of the Energy Engineering Department at a place with a lot of free space around, there were no strict dimension limitations. Dimensions were usually chosen corresponding to raw products that can be bought.

The medium flowing trough the measuring chamber is a mixture of air and water. Additionally, the test facility will use hot steam as the flowing medium in the future. On that account, all metal parts were made of stainless steel.

The nozzle itself consists of two sections. A confuser that provides a better supply of the flowing medium in the nozzle and a diffuser that serves for a better outflow of the medium. The confuser section also causes an acceleration of the medium, which is a vital effect for tearing away of water droplets. As mentioned previously, there is an airfoil in the nozzle channel from which droplets tear away.

The measuring chamber is equipped with two large glass windows for observing the tearing away process and the flow as such. Camcorders make records through the windows. If needed in the future research, one window can be replaced by some measuring probe and some other phenomena can be studied.

6.6 Specific design of the measuring chamber

6.6.1 Assembly

The measuring chamber (wind tunnel) itself consists of several pieces. The assembly is depicted in Fig. 36 (the drawing of the assembly is Appendix 2).

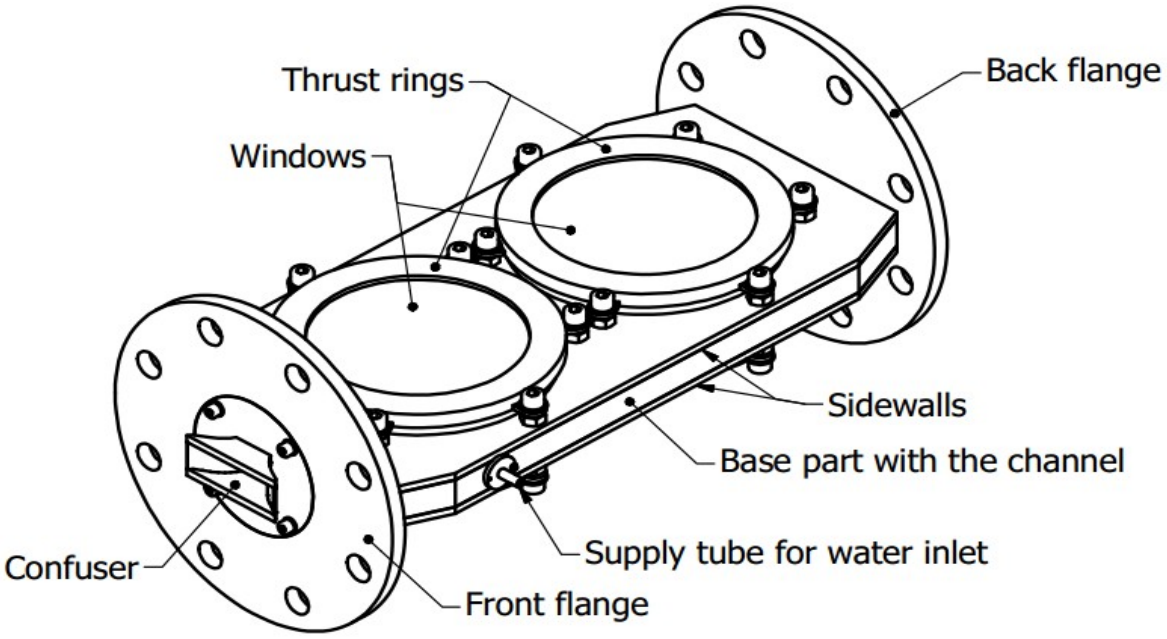

Figure 36: Assembly of the measuring chamber

The base part is made of a rectangular rod in which the channel is cut. Flanges on both sides and sidewalls are welded to the base part (the weldment is Item 1 in the drawing). There are two glass windows (Item 18) placed in housing tubes on each sidewall. The gap between the windows and inner surfaces of the housing tubes are sealed by O-rings. The windows are held by thrust rings (Item 2) bolted to the sidewalls. The first window is meant for observing the tearing away process, the second one chiefly for another research, nevertheless, it can be used for observing consequent development of the air-water mixture flow in the channel. The airfoil (Item 7) is held in the channel by supporting and coupling pins (Item 4 and 6) that are inserted through holes in sides of the base part. The pins are sealed by O-rings, too. There is a hole through the whole supporting pin that is used for inserting a supply tube (Item 5). The exceeding section of the supply tube is used as a water inlet. The confuser (Item 3) is made as a single part and it is bolted to the front flange.

6.6.1.1 Description of the welding and assembling process

At first, the base part and the sidewalls were connected and their mutual position was fixed by dowels. This was crucial to do before cutting the channel because the base part fell into two pieces after the cutting process and the dowels provided the possibility of the exact assembling. After the channel was cut, the sidewalls were welded to the base part in order to obtain a covered channel. The weldment was completed by welding the housing tubes for the windows, nuts for attaching the thrust rings and flanges on both ends.

Meanwhile, the confuser might be welded together. It consisted of two pieces of sheet metal for top and bottom part, two other pieces of bent sheet metal for side parts and a small flange for bolting to the front flange of the previously mentioned weldment. At first,

all four pieces of sheet metal were welded together. Since the side parts were made of sheet metal with the thickness of only 1 mm, spot welds were used at first so that the bent sheets keep their shapes. After that, chinks between sheets were sealed by continuous welds. The small flange was welded in the end.

The last weldments that was needed to be done were the thrust rings. Small fastening plates were welded to the outer surface of hoops. Six plates were attached to each hoop in a regular circular pattern.

Before the assembling process itself, some other adjustments were necessary. At first, the confuser was bolted to the front flange so that the hole in this flange could be manually filed in the special shape that provided a continuous connection of the confuser cavity and the channel in the base part. After that, these parts together forms the whole nozzle. Then, the confuser could be removed and supporting pins were inserted into holes in the base part. Their positions were secured using proper bolts and dowels. Subsequently, supply tubes were inserted in the pins. The pins and tubes were aligned according to their ends that interfered in the channel. Afterwards, each pin and tube were welded together at the other end of the pin. Thus, their mutual positions were fixed and ends interfering in the channel were manually filed off so that the channel in the base part was not disrupted. Then, the weldments of pins and tubes were dismounted.

After all these preliminary actions, assembling could be carried out. At first, the coupling pins and dowels were pressed in prepared holes in the weldments of the supporting pins and supply tubes. Then, O-rings were put in grooves on the surface of the supporting pins. The airfoil was placed in the channel, and its position was secured by the coupling pins and dowels pressed in the weldments the supporting pins and supply tubes that were carefully inserted into holes in the base part. Each supporting pins was secured by the bolt and dowel. Other O-rings were put in grooves in the housing tubes, subsequently the glass windows were inserted in the housing tubes and the thrust rings were bolted to the sidewalls so that the windows were secured in their position. The confuser was bolted to the front flange eventually.

6.6.2 Specification of individual components

6.6.2.1 Nozzle shape

As indicated previously, the nozzle consists of several parts. Although it is assembled of several pieces, the shape of the nozzle was designed as a seamless element. The first part of the nozzle is the convergent confuser. The cross section of the confuser gradually decreases down to the set rectangular cross section 15x20 mm. After that, the divergent diffuser follows. Three different shapes of the nozzle, that are shown in Fig. 37, were designed and subsequently flows through them were simulated.

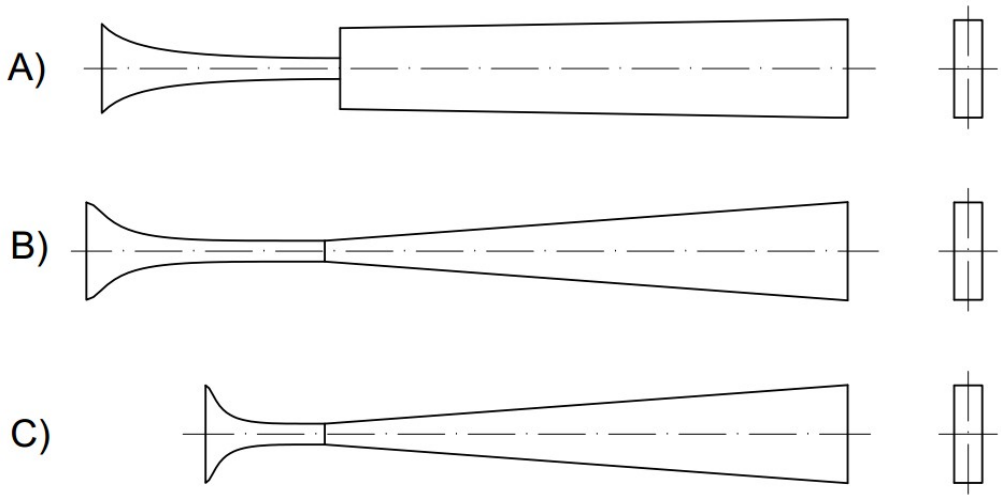

Figure 37: Three nozzle designs

Nozzle A) was designed so that the gradient of the flow velocity was constant. The diffuser part was not included in the nozzle. The absence of the diffuser emerged to be unsuitable due to vortexes, caused by the sudden change of the shape, that affect the rest of the flow. The confuser did not provide the sufficient flow acceleration either. Therefore, two other designs were made. Both nozzle B) and C) were designed according to Vitoshinski theory, only the length parameter was different. They both were equipped with the same diffuser. The diffuser cross section gradually increases up to the initial dimensions of the channel that are 70x20 mm. It defines the diffuser angle of approximately 9°. Simulations did not show any significant difference between flows in these two nozzles. Nozzle C) was chosen chiefly for its dimensions that provide cheaper manufacturing and easier assembling.

The nozzle shape is not ideal, the diffuser section could be designed with more precision, for example. The performed shape is nevertheless sufficient for first testing. Moreover, the exact design and calculation of the nozzle shape is beyond the scope of the thesis.

The flow speed of air in the narrowest part of the nozzle will not reach the supersonic speed of air at given conditions (approximately 316 m/s), nevertheless it is expected to be about 200 m/s. Moreover, the airfoil will be inserted in the channel in close proximity to the narrowest part thus the cross section of the channel at this place decreases and the flow speed increases. The supersonic flow will most likely not be reached either but the exact flow speed will not be ascertain until the operation.

It is intended to use hot steam instead of the separate supply of air and water in future projects. Due to the different feed system, the supersonic speed will be probably reached in the case of hot steam. The supersonic speed will be in the nozzle before the airfoil. There is an assumption that the airfoil will cause shock waves and there will be a subsonic speed behind the airfoil again. However, it will be a part of consequent research.

6.6.2.2 Base part

The base part is made of a rectangular rod. The width of the rod was 200 mm, height 20 mm and length 420 mm. The material of the base part is 1.4301, which is stainless steel with the yield strength σ_y = 210 N/mm^2. This steel is readily weldable and machinable. The special shaped channel was cut in the base part. After cutting, the sidewalls were welded to the base part and subsequently the hole with the diameter of 15 mm was drilled through the base part from the side. The hole is needed for the supporting pins that bear the airfoil.

6.6.2.2.1 Analysis of the channel manufacturing process

Since the channel has a special shape, as shown in Fig. 38, a non-conventional method was used for manufacturing. These methods are controlled by computer, which enables cutting of virtually any shape. Four commonly used methods were compared in order to find out which one was the most suitable. The main criteria were the shape precision and surface roughness quality so that the flow in the channel is affected as little as possible.

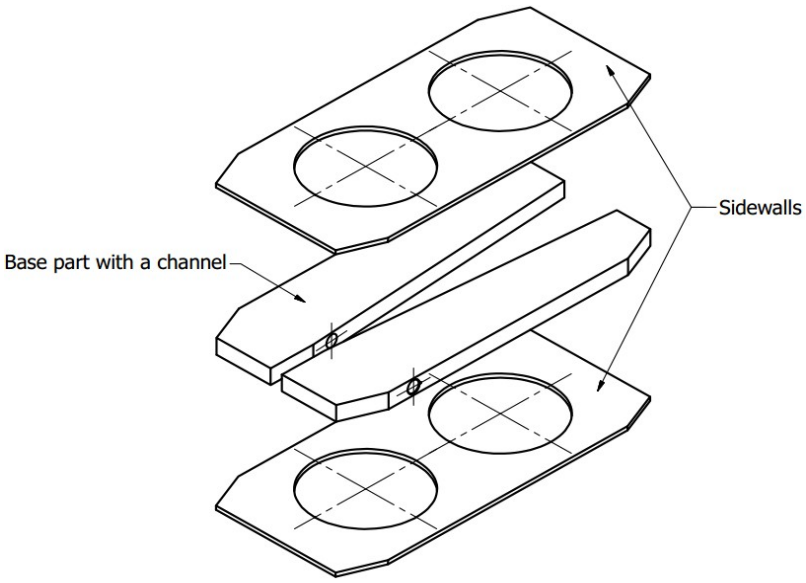

Figure 38: Core of the measuring chamber

6.6.2.2.1.1 Water jet machining

Water jet machining can use either a pure water beam or an abrasive phase (sand, glass etc.) can be added in water. The former is used for cutting soft materials (sheets and foils, wood, frozen food etc.), while the latter can cut hard materials (thick steel plates, ceramics etc.). Main advantages are very low side forces during the process, almost no heat generated in the material, low production of burrs and very low surface roughness (better than Ra 3,6). The cut precision is about 0,1mm/1m. However, this method is costly and ferrous materials need to be protected from effects of water. [25]

6.6.2.2.1.2 Laser machining

There are three types of laser cutting. In vaporization cutting, the material vaporizes due to the impact of the laser high intensity. It is suitable for non-melting materials, such as wood

or carbon. Melt and blow cutting uses an inert gas (usually nitrogen) to blow the molten material out of the cutting area. In reactive fusion cutting, the auxiliary gas reacts with the heated material that is consequently burnt. This brings energy and costs savings but the surface quality is perceptibly worse. The maximum material thickness for laser cutting is 25- 30 mm. The thickness of steel for the nozzle is close to the limit but it still should be practicable. The cut precision is about 0,1mm/1m. During the process, heat affected zones can emerge especially in thick materials. On the other hand, this method is quick, without side forces and the surface roughness is low (best Ra 3,6). For a common application in mechanical engineering, it has a very favourable quality-price ratio. [26], [27]

6.6.2.2.1.3 Plasma machining

The material is melted due to very high temperatures that are caused by a molecule decomposition during passing an electric arc. The arc is held between a non-melting cathode made of Wolfram and an anode which is often the cut material. A cutting gas is blown trough the nozzle, its molecules are ionized and a plasma is created. As the cutting gas can be used air, nitrogen or mixture of argon and hydrogen. An auxiliary gas is supplied to protect both plasma and cutting area from the influence of the atmosphere. Argon or nitrogen are used as the auxiliary gas. Plasma cutting is applicable for materials thicker than 120 mm, the surface roughness is decent (about Ra 6,3). Disadvantages are a rather broad area affected by heat and noisy operation but these can be suppressed utilizing plasma cutting under water. Also, cut sides of the material are slightly skewed. The cut precision is about 0,25mm/1m. [28], [29]

6.6.2.2.1.4 Wire electrical discharge (WED) machining

The material is removed due to an electrical discharge between electrodes. The cut material is an anode and the wire is a cathode. The electrical discharge causes melting and subsequent evaporation of the material. The whole process takes place in a dielectric liquid, which is a liquid with a high electric and thermal resistance. The cut material must be conductive. The heat affected area is very small due to a pulse character of the electrical discharge. The thickness of the material can be even 300 mm. The surface roughness is very low (about Ra = 0,2) and the shape precision can be 0,05mm/1m. The perpendicularity of cut sides is almost perfect. However, this method is costly. [30], [31]

There are other methods for material cutting based on other physical principles (ultrasonic or electron beam machining), however, they are either outdated or not easy accessible in the Prague region.

The direct comparison of described four methods for machining of the nozzle channel is given in Tab. 12. Methods were ordered according the suitability. Number 1 means the best and number 4 the worst variant.

	Water jet machin.	Laser machin.	Plasma machin.	WED machin.
Surface roughness	2	3	4	1
Shape precision	2-3	2-3	4	1
Perpendicularity of cut surfaces	3	2	4	1
Costs	3	2	1	4

Table 12: Comparison of manufacturing methods' suitability for machining of the channel

6.6.2.2.1.5 Conclusion

As mentioned previously, the quality of the cut surfaces and the shape precision of the channel is preferred to high costs. From this point of view, wire electrical discharge machining is the best variant in spite of the fact that it can be twice as expensive as water jet machining and up to tenth times more expensive than laser machining.

6.6.2.3 Sidewalls

Sidewalls are made of sheet metal. The thickness of the plate is 5 mm. The width and length are the same as base part's dimensions which are 200 mm (width) and 420 mm (length). Two holes with the diameter of 135 mm for glass windows were cut in each sidewall. The material is stainless steel 1.4301 again. Two sidewalls were made and subsequently welded to the base part.

6.6.2.4 Flanges

Two blind flanges DN 100, PN 16 were bought. Dimensions of the flange are given according to the diameter nominal (DN) and pressure nominal (PN). The outer diameter of each flange is 220 mm, the number of holes is 8 and their diameter is 18 mm, which defines bolts M16. The pressure nominal determines the maximal pressure in bars that the flange withstands. In the front flange, the rectangular hole 14x20 mm was cut and subsequently filed in the special shape during assembling, which provides a continuous connection of the confuser and base part channel. In the back flange, the simple rectangular hole 70x20 mm is cut. The material of both flanges is stainless steel 1.4301. The flanges were welded to the weldment of the base part and sidewalls.

6.6.2.5 Housing tubes

Housing tubes used for placing glass windows are made of a round rod. The outer diameter of the rod is 160 mm. A hole had to be drilled. The diameter of the hole is 135,2 mm because of O-rings. Two grooves for O-rings were cut as well. The height of the housing tubes is 14 mm, which ensures that glass windows are held firmly in their positions. The material of the tubes is stainless steel 1.4301. The housing tubes were welded on sidewalls of the nozzle.

6.6.2.6 Airfoil

The airfoil, which is shown in Fig. 39, is placed behind the narrowest place in the channel. Water is introduced through the narrow groove in the airfoil on its surface in order to create a water film so that a tearing away process can be captured by camcorders. The shape of the airfoil corresponds to NACA 0008. On both sides, two holes were drilled so that the airfoil can be attached between two supporting pins using dowels. The material is stainless steel 1.4301 again.

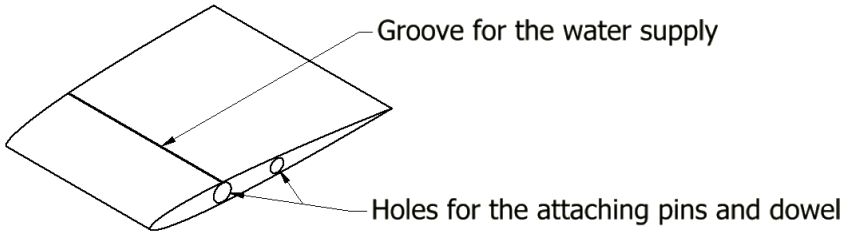

Figure 39: Airfoil

6.6.2.7 Supporting pins

Supporting pins are made of a round rod. The outer diameter of the rod was 22 mm, which was subsequently machined to the diameter of 15 mm except for a 3 mm thick shoulder at the end. The hole with the diameter of 6 mm for the supply tube was drilled through the whole pin. Length of the supporting pin is 95 mm including the shoulder. There were made two holes in the shoulder. One of them is meant for the dowel with the diameter of 1,5 mm that ensures the exact position, the other one is meant for the bolt M1,6 that secures the pin in the axial direction. Two grooves for O-rings were made in the shank of the pin. A hole was drilled in the front surface of the pin. The hole is used for the dowel with diameter of 1,5 mm that attaches the airfoil. The material of the pins is stainless steel 1.4301 again.

6.6.2.8 Supply tubes

Supply tubes are made of the tube with the outer diameter of 6 mm and the wall thickness of 2 mm. On one end, the hole was widened to the diameter of 2,5 mm in the length of 5 mm, which is meant for the coupling pin attaching the airfoil. The length of the supply tube is 110 mm. The supply tube is inserted in the supporting pin. The tube exceeds the pin intentionally so that a water supply can be connected to it. During assembling, the supply tube was welded to the supporting pin and their ends were filed so that they corresponds to the shape of the channel in the base part. The material of the supply tubes is stainless steel 1.4301.

6.6.2.9 Coupling pin

A round rod was used for manufacturing coupling pins. The diameter of the rod was 3 mm. The pin's length is 5,2 mm and it has two sections with different diameters. The wider section with the diameter of 2,5 mm is pressed in the supply tube, while the thinner section

with the diameter of 2 mm is inserted in the airfoil. A small hole for water flow was drilled through the pin. The coupling pins are also made of stainless steel 1.4301.

6.6.2.10 Glass windows

Round shaped glass windows with the diameter of 135 mm and the thickness of 20 mm were bought. Windows are made of resistant optical glass BK7 with a special coating preventing from light reflection, which was necessary in order to capture a good image for the analysis. The glass windows are placed in the housing tubes and secured by the thrust rings.

6.6.2.11 O-rings

O-rings are used for sealing the interface between the glass windows and inner diameter of the housing tubes and the interface between the hole in the base part and supporting pins. O-rings have two characteristic dimensions which are the inner diameter d_i and the diameter of the ring d_s as one can see in Fig. 40. The recommendation for O-rings is to choose as large cross section of the ring as possible.

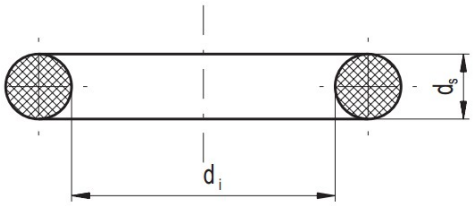

Figure 40: O-ring characteristics dimensions

6.6.2.11.1 The interface between glass windows and housing tubes

The glass windows have the outer diameter of 135 mm, which is also the inner diameter of the O-ring. The ring diameter of 3,5 mm was chosen according to rough recommendations. The cross section is not as large as possible but the pressure in the measuring chamber is not very high. Moreover, two O-rings in a row are used.

The depth of the groove for this O-ring is 2,7 mm and the width is 4,5 mm. The gap between sealed surfaces can be 0,25 mm at the maximum for such a low pressure. Therefore, the inner diameter of the tube is 135,2±0,1 mm, which provides both the tightness and easy assembling.

The compression of the static strained O-ring with the cross section of 3,5 mm should lie within interval from 12 to 26% for its proper function. The check calculation is performed in Eq. 47.

$$c = \frac{d_s - l}{d_s} = \frac{3{,}5\,mm - 2{,}7\,mm}{3{,}5\,mm} = 22{,}9\,\% \qquad (47)$$

The compression met the condition and O-rings fulfills their functions.

6.6.2.11.2 The interface between the base part and supporting pins

Grooves for O-rings were made on the shank surface of the supporting pin. The O-ring diameter of 1,5 mm was chosen. The depth and width of the groove for such an O-ring is 1,15 mm and 1,9 mm, respectively. Since the outer diameter of the pin is 15 mm, the diameter at the place of the groove is 12,7. The inner diameter of the O-ring is 12,5 mm, which is right since the inner diameter should be equal or smaller than the diameter of the groove.

The gap between sealed surfaces can be 0,25 mm. Therefore, the holes in the base part have the exact diameter of $15^{+0,1}_{+0}$ mm and the supporting pins have the diameter of $15^{+0}_{-0,2}$ mm, which ensures both tightness and assembling.

In this case, the compression of the O-ring should be within interval from 12,5 to 29 %, which is checked in Eq. 48.

$$c=\frac{d_s-l}{d_s}=\frac{1,5\,mm-1,15\,mm}{1,5\,mm}=23,3\,\% \qquad (48)$$

The condition is met and such O-rings can be used.

6.6.2.12 Hoops of thrust rings

Hoops are made of the round rod with the diameter of 170 mm. The piece of the rod with the thickness of 9 mm was used. The outer diameter was machined to 167 mm at first. Afterwards, the hole with the diameter of 126 mm was drilled. Subsequently, the hole of the diameter 161 mm was machined, but this hole did not go through so that a kind of shoulder similar to the union nut structure was created. The depth of the hole is 6 mm. The material of the hoops is stainless steel 1.4301.

6.6.2.13 Fastening plates of thrust rings

Fastening plates are made of sheet metal with the thickness of 3 mm. The whole shape of the plate was cut by laser including the hole for the bolt M8. The fastening plates were welded to the hoops and resulted thrust rings are used to secure glass windows in their positions. The material is stainless steel 1.4301 again.

6.6.2.14 Confuser

The confuser is a weldment consisting of four sheet metal pieces and a flange. The bottom and top part were made of sheet metal with the thickness of 5 mm. These two pieces were only cut, while two other pieces (side parts) were bent furthermore. The sheet metal thickness of the side parts was 1 mm. All four pieces were welded together to form a funnel eventually.

The flange is made of sheet metal with the thickness of 2 mm. The outer diameter of the flange is 94 mm. Four holes for bolts M5 were drilled in the flange. In the middle of the flange, a hole for the end of the confuser funnel was cut. The confuser flange and the confuser funnel were welded together. The material of all parts is of stainless steel 1.4301.

6.7 Strength calculations of the test section

Parts of the test facility that are very stressed by the pressure were checked by calculations. The highest pressure is in the settling chamber, and thus strength calculations of the tube and welds of the chamber were carried out. There were many others welds that could have been checked, such as welds connecting the measuring chamber. However, these welds are exposed to a significantly lower pressure due to expansion of compressed air, hence their check calculations were not necessary.

6.7.1 Settling chamber

The settling chamber consists of a tube and two caps. The outer diameter of the tube is 306 mm, thickness of the wall is 3 mm and length is about 500 mm. The caps have the same outer diameter and wall thickness naturally. They were welded to ends of the tube. The material of both tube and caps is stainless steel 1.4301. The air pressure in the chamber is considered to be 6 bars and the temperature is assumed to be the room temperature of 25°C.

6.7.1.1 The tube of the settling chamber

The chamber is stressed by the internal pressure and it can be calculated as a thin-walled vessel because the wall thickness is much smaller then the inner diameter of the tube. It is said that the ratio of the radius and wall thickness must be greater than 10. This condition is checked in Eq. 49.

$$\frac{r}{s}=\frac{150}{3}=50>10 \tag{49}$$

There are three main stresses in the wall – tangential, axial and radial. Calculations of them are carried out in Eq. 50, 51 and 52.

$$\sigma_t=\frac{p\cdot r}{s}=\frac{6\cdot 10^5\cdot 0{,}15}{3\cdot 10^{-3}}=30\,N/mm^2 \tag{50}$$

$$\sigma_a=\frac{p\cdot r}{2\cdot s}=\frac{6\cdot 10^5\cdot 0{,}15}{2\cdot 3\cdot 10^{-3}}=15\,N/mm^2 \tag{51}$$

$$\sigma_r=-p=-0{,}6\,N/mm^2 \tag{52}$$

In order to gain the equivalent tensile stress, von Mises yield criterion was used. The calculation is in Eq. 53.

$$\sigma_v = \frac{\sqrt{2}}{2} \cdot \sqrt{(\sigma_t - \sigma_a)^2 + (\sigma_a - \sigma_r)^2 + (\sigma_r - \sigma_t)^2}$$

$$\sigma_v = \frac{\sqrt{2}}{2} \cdot \sqrt{(30-15)^2 + [15-(-0{,}6)]^2 + (-0{,}6-30)^2} = 26{,}5\, N/mm^2 \quad (53)$$

The yield strength of the material 1.4301 is σ_y = 210 N/mm^2. The factor of safety is k = 1,5 in the case of a pressure vessel. The permissible stress is calculated in Eq. 54.

$$\sigma_p = \frac{\sigma_y}{k} = \frac{210\, N/mm^2}{1{,}5} = 140\, N/mm^2 \quad (54)$$

The permissible stress σ_p is greater than the equivalent tensile stress σ_v $(140\, N/mm^2 > 26{,}5\, N/mm^2)$, which means that the tube withstands the internal pressure of 6 bars.

6.7.1.2 Weld between the tube and cap

The impact of the pressure on ending caps of the settling chamber causes a tensile stress in weld joints connecting the tube part and caps of the chamber. This stress is in the transverse direction to the welds.

At first, a force caused by the pressure in the transverse direction was calculated as shown in Eq. 55.

$$F = p \cdot S = 6 \cdot 10^5 \cdot \frac{\pi}{4} \cdot (0{,}3^2) = 42{,}4\, kN \quad (55)$$

The tensile stress was calculated following Eq. 56.

$$\sigma_{tn} = \frac{F}{\frac{\pi}{4} \cdot (D_w^2 - d_w^2)} = \frac{42{,}4 \cdot 10^3}{\frac{\pi}{4} \cdot (0{,}306^2 - 0{,}3^2)} = 14{,}85\, N/mm^2 \quad (56)$$

The conversion coefficient α_t for groove welds stressed by transverse loading was used to obtain a modified tensile stress that could be compared to the permissible stress of the base material as shown in Eq. 57.

$$\sigma_m = \frac{\sigma_{tn}}{\alpha_t} = \frac{14{,}85\, MPa}{0{,}7} = 21{,}21\, N/mm^2 \quad (57)$$

The base material is stainless steel 1.4301 again and the permissible stress σ_p that was calculated in Eq. 54 is greater than modified tensile stress σ_m $(140\, N/mm^2 > 21{,}21\, N/mm^2)$. Therefore, welds withstand the internal pressure of 6 bars.

6.7.2 The connecting tube

The settling chamber is connected with the measuring chamber by the tube with the outer diameter of 114,3 mm and wall thickness of 2 mm. This connecting tube is exposed to the same pressure and temperature as the settling chamber. The calculation was performed in the same way as show Eq. 58-62.

$$\frac{r}{s}=\frac{55,15}{2}=27,58>10 \tag{58}$$

$$\sigma_t=\frac{p\cdot r}{s}=\frac{6\cdot 10^5\,Pa\cdot 0,055\,m}{2\cdot 10^{-3}\,m}=16,5\,N/mm^2 \tag{59}$$

$$\sigma_a=\frac{p\cdot r}{2\cdot s}=\frac{6\cdot 10^5\,Pa\cdot 0,055\,m}{2\cdot 2\cdot 10^{-3}\,m}=8,25\,N/mm^2 \tag{60}$$

$$\sigma_r=-p=-0,6\,N/mm^2 \tag{61}$$

$$\sigma_v=\frac{\sqrt{2}}{2}\cdot\sqrt{(16,5-8,25)^2+[8,25-(-0,6)]^2+(-0,6-16,5)^2}=14,8\,N/mm^2 \tag{62}$$

The condition for using the calculation of a thin-wall vessel was met as shows Eq. 58. The material of the connecting tube is 1.4301 again and therefore the permissible stress has the same value that was calculated in Eq. 54. From the comparison of the permissible stress σ_p and the equivalent tensile stress σ_v $\left(140\,N/mm^2>14,8\,N/mm^2\right)$ is obvious that the connecting tube withstands the pressure as well.

6.7.3 Flange joint

Flange joints of the measuring chamber could be calculated, too. However, it was not necessary. Flanges PN 16 were bought, which indicates that the flange could be safely used up to the pressure of 16 bars. The maximal pressure in the test facility is 6 bars, which is deep below the limit.

6.8 Conclusion

The measuring chamber, which is in this particular case a special type of a wind tunnel, is designed with respect to several requirements. The former idea of reaching the supersonic flow speed of air through the chamber turned out to be impossible in given conditions. Nevertheless, there is still expected the flow speed about 200 m/s and that was assumed to be sufficient for the first phase of the chamber development.

The chamber is manufactured with emphasis on quality regardless higher costs. It should provide the best possible conditions for the air flow and other processes taking place so that they would not be disturbed.

Last but not least, the measuring chamber is designed as an individual component of the test facility. It means that the chamber can be replaced by another one with a different internal arrangement or even by some other device for studying different phenomena.

7 Conclusion

This thesis was written as a part of extensive research taking place at the Department of Energy Engineering. This research is focused on improvements of efficiency, reliability, and lifetime of steam turbines.

Besides other things, coarse droplets are responsible for a decrease of mentioned turbine properties. They occur at last stages of low pressure steam turbines but their quantity, dimensions, and exact movement velocities has not been sufficiently examined yet. Since many methods has been proved to be unsuitable for an investigation of coarse droplets, photogrammetry was suggested. One disadvantage of the application of this method is a large number of pictures that are taken and that have to be analysed.

A basic version of a computer program for an automatic image analysis was developed in the first part of the thesis. It was tested on several images containing objects of a different size and shape. Namely, samples of glass powder and ground coal were in the pictures. Testing proved that the program can identify and highlight objects on the image and form basic granulometry characteristics as well. Nevertheless, the program still need some improvements in order to provide more accurate and reliable results. For example, deblurring of objects in captured images, which would lead to a more accurate determination of object edges, could be implemented in the program.

After some adjustments, the program could be conveniently used for the identification of other polydisperse systems. In energy technology, there can be the analysis of polydisperse system used to acquire information about air pollution after a combustion process, for example. The knowledge of granulometry characteristics is also useful in evaluating of quality of solid fossil fuels after the milling process, especially for pulverised firing.

Within the research, a photogrammetric probe for capturing images directly in steam turbines has been developed. Before the probe will be applied in turbines, its functionality will have to be tested. A device designed in the other part of the thesis will help to verify the functionality of the probe. It is a wind tunnel for simulating and observing the tearing away process of water droplets. The wind tunnel is placed in a test facility consisting of an air tank, settling chamber and the wind tunnel (measuring chamber) itself. Water is supplied on the airfoil placed in the measuring chamber and air flowing through the chamber tears droplets away. The measuring chamber has two windows so that the process can be captured by camcorders.

It was initially thought that the flow speed in the wind tunnel will be supersonic, however it would lead to very small dimensions of the channel. Therefore, the idea was abandoned regarding this first testing device and the subsonic speed of about 200 m/s is expected in the channel. The shape of the contracting part of the channel was designed according to Vitoshinski theory. The airfoil is placed close behind the narrowest cross section of the

channel so that tearing away is caused by a very high flow speed. Moreover, the airfoil slightly decreases the cross section of the channel and thus the flow speed will increase a little. The exact flow speed will be acquired during the operation.

The measuring chamber arrangement was designed for air as the flowing medium and the separate supply of water. Nevertheless, the test facility with the measuring chamber can be used for hot steam as the flowing medium in the future, which would be a better simulation of the real process in steam turbines. A few adjustments is necessary though.

The measuring chamber can be also replaced in the test facility by another one with a different channel shape, for example, which would provide different conditions for the flowing medium. This way, some other phenomena might be examined.

The main reason for writing this thesis was a need for an identification of coarse droplets in last stages of low pressure parts of steam turbines. On that account, a basic version of a computer program that is able to identify and analyse polydisperse systems was developed. Further, the device for simulating the tearing away process of coarse droplets was designed. Firstly, it could be used for verifying the suitability of the program for analysing coarse droplets, and secondly, it should help to test the functionality of the photogrammetric probe that has been developed within research at the Department of Energy Engineering.

Sources

[1] HINDS, William C. *Aerosol technology: properties, behavior, and measurement of airborne particles*. 2nd ed. New York: Wiley, c1999, xx, 483 p. ISBN 0471194107.

[2] BARTOVSKÁ, Ludmila a Marie ŠIŠKOVÁ. Disperzní systém. *Co je co v povrchové a koloidní chemii* [online]. Praha: Vydavatelství VŠCHT Praha, 2005 [qte. 2015-09-24]. Accessible on: http://vydavatelstvi.vscht.cz/knihy/uid_es-001/hesla/disperzni_system.html

[3] Colloid. *Wikipedia: the free encyclopedia* [online]. San Francisco (CA): Wikimedia Foundation, 2001- [qte. 2015-09-24]. Accessible on: https://en.wikipedia.org/wiki/Colloid

[4] Aerosol. *Wikipedia: the free encyclopedia* [online]. San Francisco (CA): Wikimedia Foundation, 2001-, 14.9.2015 [qte. 2015-09-24]. Accessible on: https://en.wikipedia.org/wiki/Aerosol

[5] NIST/SEMATECH: e-Handbook of Statistical Methods. *NIST* [online]. 2013, 30.10.2013 [qte. 2015-10-05]. Accessible on: http://www.itl.nist.gov/div898/handbook/eda/section3/eda362.htm

[6] FAN, Liang-Shih a Chao ZHU. *Principles of gas-solid flows*. New York: Cambridge University Press, 1998, xvii, 557 p. ISBN 0521581486

[7] RAWLE, A. *Basic principles of particle size analysis* [online]. [qte. 2015-10-08]. Accessible on: http://www.rci.rutgers.edu/~moghe/PSD%20Basics.pdf

[8] JILLAVENKATESA, Ajit, Stanley DAPKUNAS a Lin-Sien H. LUM. *Particle Size Characterization: NIST Recommended Practice Guide* [online]. 2001,: 164 [qte. 2015-10-29]. Accessible on: http://permanent.access.gpo.gov/LPS58724/SP960-1.pdf

[9] ALLEN, Terence. *Powder sampling and particle size determination*. 1st ed. Boston: Elsevier, 2003, xvi, 660 p. ISBN 044451564x

[10] *How to carry out Wet Sieving* [online]. Haan, Germany: Retsch GmbH, 2005 [qte. 2015-11-22]. Accessible from: http://www.umb.no/statisk/fortek/other/retsch_wet_sieving__official_document_.pdf

[11] MINGARD, K; MORRELL R; JACKSON P. *A NATIONAL MEASUREMENT GOOD PRACTICE GUIDE: Improving the consistency of particle size measurement*. 111. Teddington: National Physical Laboratory, 2009. ISSN 1368-6550.

[12] MORSE, P.; LOXLEY A. Light microscopic determination of particle size distribution in an aqueous gel. *Drug delivery technology*. 2009, (9), [qte. 2015-11-23]. Accessible from: http://www.particlesciences.com/docs/DDT-Particle_Size_Dist-May_09.pdf

[13] LUHMANN, T.; ROBSON, S. *Close range photogrammetry: principles, methods and applications*. Dunbeath: Whittles, 2006. ISBN 18-703-2550-8.

[14] Photogrammetry. In: *Wikipedia: the free encyclopedia* [online]. San Francisco (CA): Wikimedia Foundation, 2001- [qte. 2016-01-11]. Accessible from: https://en.wikipedia.org/wiki/Photogrammetry#Stereophotogrammetry

[15] SCHENK, T. *Introduction to Photogrammetry* [online]. The Ohio State University, 2005, 1-100 [qte. 2016-01-12]. Accessible from: http://www.mat.uc.pt/~gil/downloads/IntroPhoto.pdf

[16] KLEITZ, A. and DOREY, J. M. Instrumentation for wet steam. Journal of Mechanical Engineering Science. 2004, (218), 811-842. ISSN 0954-4062.

[17] CRANE, R. I. Droplet deposition in steam turbines. Journal of Mechanical Engineering Science. 2004, (218), 859-870. ISSN 0954-4062.

[18] BARTOŠ, O., CAI X. a KOLOVRATNÍK M. *A detection of the coarse waterdroplets in steam turbines*. EPJ Web of Conferences. 2014, (67). DOI: http://dx.doi.org/10.1051/epjconf/20146702005

[19] BARTOŠ, Ondřej. Studium elektrostatického náboje kapek při expanzi v parní dýze a nízkotlakém dílu parní turbíny. Praha, 2008. Dissertation. ČVUT.

[20] KOLOVRATNÍK, Michal a Ondřej BARTOŠ. CTU Optical probes for liquid phase detection in the 1000 MW steam turbine. Int. conf. Experimental Fluid Mechanics 2014. 273-277.

[21] Wind Tunnels. *NASA* [online]. 2009 [qte. 2016-04-11]. Accessible from: http://www.nasa.gov/audience/forstudents/9-12/features/F_Wind_Tunnels.html

[22] Wind Tunnel Design. *NASA* [online]. 2015 [cit. 2016-04-11]. Accessible from: https://www.grc.nasa.gov/www/k-12/airplane/tunnozd.html

[23] Wind Tunnel Parts. *NASA* [online]. 2015 [cit. 2016-04-11]. Accessible from: https://www.grc.nasa.gov/www/k-12/airplane/tunpart.html

[24] MUZIK, T., SAFARIK, P. a TUCEK, A. Analysis of the water film behaviour and its breakup on profile using experimental and numerical methods. *Journal of Thermal Science* [online]. 2014, **23**(4), 325-331 [cit. 2016-05-27]. DOI: 10.1007/s11630-014-0713-7. ISSN 1003-2169. Accesible from: http://link.springer.com/10.1007/s11630-014-0713-7

[25] Vodní paprsek - technologie. CHPS s.r.o. – řezání vodním paprskem, řezání laserem, zpracování kovů. [online]. [qte. 2016-03-04]. Accessible from: http://www.chps.cz/vodni-paprsek/technologie

[26] Laser - technologie. CHPS s.r.o. – řezání vodním paprskem, řezání laserem, zpracování kovů. [online]. [qte. 2016-03-04]. Accessible from: http://www.chps.cz/rezani-laserem/technologie

[27] ŘASA, J. a KEREČANINOVÁ, Z. Nekonvenční metody obrábění – 5. díl. MM Průmyslové spektrum. 2008, (5), pg. 68.

[28] ŘASA, J. a KEREČANINOVÁ, Z. Nekonvenční metody obrábění – 8. díl. MM Průmyslové spektrum. 2008, (10), pg. 32.

[29] CENTRUM VZDĚLÁVÁNÍ PEDAGOGŮ ODBORNÝCH ŠKOL: Progresivní způsoby dělení materiálu ve výrobním procesu [online]. Uherský Brod: Secondary Industrial School and Business Academy Uherský Brod, 2012 [qte. 2016-03-05]. Accessible from: http://int.spsoa-ub.cz/ccv/projekty/vzdelavanipedagogu/dokumenty/skripta/skripta_vp_10.pdf

[30] BARTOŠ, P. Elektroerozivní drátové řezání. Brno, 2011. Diploma thesis.

[31] ŘASA, J. a KEREČANINOVÁ, Z. Nekonvenční metody obrábění – 2. díl. MM Průmyslové spektrum. 2007, (10), pg. 58.

List of appendices

A) Code of the program for the image analysis

B) Drawing of the measuring chamber assembly along with the bill of material

A) Code of the program for the image analysis

```
close all
clear all

I = imread('Capture_22.bmp'); % reading of the picture from the file

I2 = rgb2gray(I); % conversion of the picture to the greyscale image

% setting of a threshold and the conversion to the black and white image
threshold = graythresh(I2);
I = im2bw(I2,threshold);

figure, imshow(I) % depiction of the image

% removal of the grid lines in a horizontal position
dim = size(I2);
for i = 1:dim(1)
    j = 1;
    poc = 0;
    pom = I(i,j);
    while (j < dim(2) && pom == 0 && pom == I(i,j+1))
        j = j+1;
        poc = poc+1;
        if poc > (dim(1)/2)
            for k = 1:dim(2)
                I(i,k) = I(i-1,k);
            end
        end
    end
end

% removal of the grid lines in a vertical position
for j = 1:dim(2)
    i = 1;
    poc = 0;
    pom = I(i,j);
    while (i < dim(1) && pom == 0 && pom == I(i+1,j))
        i = i+1;
        poc = poc+1;
        if poc > (dim(2)/2)
            for k = 1:dim(1)
                I(k,j) = I(k,j-1);
            end
        end
    end
end

I = imcomplement (I); % inversion of black and white colours
figure, imshow(I)

I = bwareaopen(I,100); % removal of objects smaller than 100 pixels

I = imfill(I,'holes');  % filling of holes inside objects

[B,L] = bwboundaries(I,'noholes'); % finding of boundaries of objects
```

```
% coloration of objects and their boundaries
map = [0, 0, 0.7];
for k = 1:length(B)
    map = [map; [0, 0, 0.7]];
end
figure
img = label2rgb(L, map, [.5 .5 .5]);
imshow(img)
hold on
for k = 1:length(B)
  boundary = B{k};
  plot(boundary(:,2), boundary(:,1), 'w', 'LineWidth', 1)
end

% gaining of areas and perimeters of objects
stats = regionprops(L,'Area', 'Perimeter');

% conversion from pixels to micrometers (1 pix = 1/1056 mm)
conver = (1/1056)*1000;
for k = 1:length(stats)
    stats(k).Area = stats(k).Area*(conver^2);
    stats(k).Perimeter = stats(k).Perimeter*conver;
end

% finding of minimal and maximal areas
min = stats(1).Area;
max = 1;
area = 0;
for k = 1:length(B)
  area(k) = stats(k).Area;
  if min > area(k)
      min = area(k);
      indexmin = k;
  elseif max < area(k)
      max = area(k);
      indexmax = k;
  end
end

% highlighting of the smallest and largest objet
boundary = B{indexmin};
plot(boundary(:,2), boundary(:,1), 'y', 'LineWidth', 2)
boundary = B{indexmax};
plot(boundary(:,2), boundary(:,1), 'r', 'LineWidth', 2)

% calculation of diameters based on the areas
for k = 1:length(B)
    da(k) = sqrt(4*area(k)/pi());
end

sumda = sum(da);
da10 = sumda/length(B);

da2 = da.^2;
sumda2 = sum(da2);
da20 = sqrt(sumda2/length(B));
```

```
da3 = da.^3;
sumda3 = sum(da3);
da30 = nthroot(sumda3/length(B),3);
daS = sumda3/sumda2;

da4 = da.^4;
sumda4 = sum(da4);
daB = sumda4/sumda3;

% calculation of diameters based on the perimeters
for k=1:length(B)
    perimeter(k) = stats(k).Perimeter;
end
for k = 1:length(B)
    dp(k) = perimeter(k)/(2*pi());
end

sumdp = sum(dp);
dp10 = sumdp/length(B);

dp2 = dp.^2;
sumdp2 = sum(dp2);
dp20 = sqrt(sumdp2/length(B));

dp3 = dp.^3;
sumdp3 = sum(dp3);
dp30 = nthroot(sumdp3/length(B),3);
dpS = sumdp3/sumdp2;

dp4 = dp.^4;
sumdp4 = sum(dp4);
dpB = sumdp4/sumdp3;

% plotting of the graphs
dasort = sort(da);
areasort = sort(area);
dpsort = sort(dp);

figure
subplot(2,2,1),
    plot (area,'r.')
    xlim([0 110]);
    title('A) Object''s area - no order');
    xlabel('Object''s index k [-]')
    ylabel('Area [um^2]')
subplot(2,2,3),
    plot (areasort, '.')
    xlim([0 110]);
    title('B) Object''s area - ordered');
    xlabel('Object''s index k [-]')
    ylabel('Area [um^2]')
area2 = areasort(1:90);
subplot(1,2,2),
    plot (area2, '.')
    title('C) Object''s area - ordered, detail');
    xlabel('Object''s index k [-]')
    ylabel('Area [um^2]')
```

```
kg = [1:length(B)];
figure
    p = plot (dasort,kg/length(B), dasort,(1-kg/length(B)));
    p(1).Marker = '.';
    p(1).MarkerSize = 8;
    p(2).Marker = '.';
    p(2).MarkerSize = 8;
    xlabel('Object''s diameter d_a [um]')
    ylabel('F(d_a), S(d_a) [-]')
    legend('F(d_a)','S(d_a)')

% writing of the characteristics
pocet = length(B);
formatSpec_pocet = 'Number of objects: %d.';
str_pocet = sprintf(formatSpec_pocet,pocet);

formatSpec_min = 'The smallest area: %d um^{2}.';
str_min = sprintf(formatSpec_min,round(areasort(1)));

formatSpec_max = 'The largest area: %d um^{2}.';
str_max = sprintf(formatSpec_max,round(areasort(length(B))));

formatSpec_mean = 'The avarage area value: %d um^{2}.';
str_mean = sprintf(formatSpec_mean,round(mean(area)));

formatSpec_median = 'The median value: %d um^{2}.';
str_median = sprintf(formatSpec_median,round(median(area)));

str_da10 = sprintf('d_{a[1,0]}: %d um.', round(da10));
str_da20 = sprintf('d_{a[2,0]}: %d um.', round(da20));
str_da30 = sprintf('d_{a[3,0]}: %d um.', round(da30));
str_daS = sprintf('d_{aS}: %d um.', round(daS));
str_daB = sprintf('d_{aB}: %d um.', round(daB));
str_dp10 = sprintf('d_{p[1,0]}: %d um.', round(dp10));
str_dp20 = sprintf('d_{p[2,0]}: %d um.', round(dp20));
str_dp30 = sprintf('d_{p[3,0]}: %d um.', round(dp30));
str_dpS = sprintf('d_{pS}: %d um.', round(dpS));
str_dpB = sprintf('d_{pB}: %d um.', round(dpB));

figure
axis off
text (0.05,0.9, str_pocet)
text (0.05,0.8, str_min)
text (0.05,0.75, str_max)
text (0.05,0.65, str_mean)
text (0.05,0.6, str_median)
text (0.05,0.5, str_da10)
text (0.05,0.45, str_da20)
text (0.05,0.4, str_da30)
text (0.05,0.35, str_daS)
text (0.05,0.3, str_daB)
text (0.4,0.5, str_dp10)
text (0.4,0.45, str_dp20)
text (0.4,0.4, str_dp30)
text (0.4,0.35, str_dpS)
text (0.4,0.3, str_dpB)
```